ACADEMIC PRESS

Available online at www.sciencedirect.com

SCIENCE DIRECT®

Journal of Sound and Vibration 264 (2003) 605–637

JOURNAL OF SOUND AND VIBRATION

www.elsevier.com/locate/jsvi

Dynamic response of doubly curved honeycomb sandwich panels to random acoustic excitation. Part 2: Theoretical study

P.R. Cunningham[a,*], R.S. Langley[b], R.G. White[a]

[a] *School of Engineering Sciences, Aeronautics and Astronautics, University of Southampton, Highfield, Southampton, Hampshire SO17 1BJ, UK*

[b] *Department of Engineering, University of Cambridge, Trumpington Street, Cambridge CB2 1PZ, UK*

Received 6 August 2001; accepted 26 June 2002

Abstract

In this paper a single-degree-of-freedom model is developed to predict the dynamic response of an acoustially excited doubly curved sandwich panel. Three variants of the model are investigated, based on differing assumptions regarding the spatial distribution of the applied loading. When the loading is assumed to be uniform then the model reduces to the Miles approach, and when the loading is assumed to conform to the structural mode shape then the method is very similar to the Blevins approach. The third variant involves a more detailed consideration of the travelling wave characteristics of the applied loading, and this is found to give much improved agreement with experimental results obtained in a progressive wave tube facility. In addition, an approach using the finite element method is presented in which the response to grazing incidence excitation is computed, and this is also found to yield good agreement with the experimental results.

1. Introduction

Composite materials are becoming more widespread in the construction of aircraft secondary and tertiary structures due to the need for low weight and hence reduced fuel costs and greater range. Sandwich panels are one particular type of composite construction that have many applications such as in flooring panels, fairings, flap construction, tail-cones, and engine intake barrel panels.

Following an examination of the current design guidelines [1] adopted for composite structures, it is apparent that there is a need for more advanced response prediction models for doubly curved

*Corresponding author. Tel.: +44-23-8059-4887; fax: +44-23-8059-3058.

E-mail address: prc1@soton.ac.uk (P.R. Cunningham).

0022-460X/03/$ - see front matter
PII: S0022-460X(02)01211-7

composite honeycomb sandwich structures subject to random acoustic excitation. Various investigations have been conducted in the past on metallic and composite structures [1–6]. These studies have involved the comparison of measured and predicted stresses/strains, and in general the results have indicated a bias in which estimates appear to be greater than measurements by a factor of about two [5].

In this paper, several approaches are presented for predicting the dynamic response of a set of four doubly curved, composite honeycomb sandwich panels. A complementary experimental investigation was also carried out to determine the strain response of a set of doubly curved test panels to broadband random acoustic excitation using a PWT facility, and details of this work can be found in Part 1 of this study [7].

Various methods of predicting the dynamic response of doubly curved composite honeycomb sandwich structures to random acoustic excitation, are presented in this paper. The first is based on the single-degree-of-freedom (s.d.o.f.) approach, where the modes of vibration are assumed to be lightly damped and well separated. The predominant mode of vibration is therefore treated as a s.d.o.f. system. The equations for a system subject to random excitation are developed in this paper, and are applied to the case of the doubly curved sandwich panels. Three different variants of the method are investigated, which involve estimating the spatial characteristics of the pressure loading. The finite element model, presented in a recent publication [8], was then used to provide the modal inputs to the equations from which the r.m.s. response was calculated. The results are compared with the r.m.s. measured response as presented in Part 1 of this study. Comparisons are also made with the solution using Blevins method [6]. Finally, the finite element model is used to predict the response by considering the load as a series of travelling harmonic waves at grazing incidence to the surface of the structure. The harmonic solution is then used, together with the measured pressure spectrum, to arrive at an estimate of the strain power spectral density (PSD), which is again compared with the measured strain PSD. Conclusions are drawn concerning the advantages and disadvantages of the three dynamic response prediction methods, and recommendations are made for further work.

2. The single-degree-of-freedom approximation

At low frequencies the modes of vibration of a structure tend to have a frequency spacing that is large in comparison to the modal bandwidth. In this case it is reasonable to neglect any resonant response overlap that might arise between the modes through the action of damping, and the dynamics of a single mode of vibration can be considered in isolation of the other modes. The problem formulation and solution procedure outlined in this section are based on the standard methods of linear random vibration analysis (see for example Refs. [9,10]). The response $u(\mathbf{x}, t)$ associated with a single mode of vibration (say the nth mode) can be written in the form

$$u(\mathbf{x}, t) = w_n(t)\phi_n(\mathbf{x}), \tag{1}$$

$$\int_{A_0} m\phi_n^2(\mathbf{x})\,\mathrm{d}\mathbf{x} = 1, \tag{2}$$

where $\mathbf{x} = (x_1 x_2)$ represents the spatial co-ordinates of a point on the structure, $w_n(t)$ is the modal amplitude, and $\phi_n(\mathbf{x})$ is the mode shape, which is taken to be scaled to unit generalized mass in accordance with Eq. (2), where m is the mass per unit area and A_0 represents the mid-plane surface. For a curved panel, $u((x), t)$ is taken to be the normal component of the panel displacement, and x_1 and x_2 are curvilinear co-ordinates that lie in the panel mid-surface. In this case the left-hand side of Eq. (2) should strictly include the generalized mass arising from the tangential displacements, although for bending type modes (of interest here) these terms will be very small. The equation of motion that governs the amplitude $w_n(t)$ has the form

$$\ddot{w_n} + 2\zeta_n \omega_n \dot{w_n} + \omega_n^2 w_n = F_n(t), \tag{3}$$

where ω_n is the natural frequency, ζ_n is the non-dimensional viscous damping ratio, and $F_n(t)$ is the generalized force, given by

$$F_n(t) = \int_{A_0} p(\mathbf{x}, t)\phi(\mathbf{x})\,\mathrm{d}\mathbf{x}. \tag{4}$$

Here $p(\mathbf{x}, t)$ is a random distributed pressure, and it is clear that the power spectral density $S_{FF}(\omega)$ of $F_n(t)$ will depend on the statistical properties of $p(\mathbf{x}, t)$. In general,

$$S_{FF}(\omega) = \int_{A_0}\int_{A_0} S(\mathbf{x}, \mathbf{x}', \omega)\phi_n(\mathbf{x})\phi_n(\mathbf{x}')\,\mathrm{d}\mathbf{x}\,\mathrm{d}\mathbf{x}', \tag{5}$$

where

$$S(\mathbf{x}, \mathbf{x}', \omega) = \left(\frac{1}{2\pi}\right)\int_{-\infty}^{\infty} E[p(\mathbf{x}, t)p(\mathbf{x}', t+\tau)]\mathrm{e}^{-\mathrm{i}\omega\tau}\,\mathrm{d}\tau \tag{6}$$

is the cross-spectrum of the pressure at the points $\mathbf{x}$ and $\mathbf{x}'$. The present work is concerned with the development of a straightforward approximate method of predicting the system response, and to this end it is helpful to consider a special case of Eq. (6). In general, the pressure can be fully random in both time and space; a more restricted situation arises when the spatial pressure distribution can be deduced from the knowledge of the pressure at a single reference point, i.e., a frequency-dependent transfer function $H(\mathbf{x}, \omega)$ exists between the pressure at the point $\mathbf{x}$ and the pressure at the reference point. In this case Eq. (6) becomes

$$S(\mathbf{x}, \mathbf{x}', \omega) = H(\mathbf{x}, \omega)H^*(\mathbf{x}', \omega)S_{pp}(\omega), \tag{7}$$

where $S_{pp}(\omega)$ is the spectrum of the reference pressure. Specific examples of this type of loading, which are discussed in more detail in the follow sub-sections, are: uniform pressure loading $H(\mathbf{x}, \omega) = 1$, a pressure distribution matched to the vibration mode shape $H(\mathbf{x}, \omega) = \phi_n(\mathbf{x})$, and finally travelling wave excitation $H(\mathbf{x}, \omega) = \exp(-\mathrm{i}k_1 x_1 - \mathrm{i}k_2 x_2)$, where k_1 and k_2 are the appropriate wavenumbers. If Eq. (7) is applicable then the spectrum of the generalized force, Eq. (5), becomes

$$S_{FF}(\omega) = \left|\int_{A_0} H(\mathbf{x}, \omega)\phi_n(\mathbf{x})\,\mathrm{d}\mathbf{x}\right|^2 S_{pp}(\omega). \tag{8}$$

If the system is lightly damped then the excitation can be approximated to white noise, at least over the modal bandwidth, and Eq. (3) can be solved to yield the following closed-form expression

for the mean squared modal response [10]:

$$\sigma_w^2 = \frac{\pi S_{FF}(\omega_n)}{4\zeta_n \omega_n^3}. \tag{9}$$

Various special cases of Eq. (9) are now considered, arising from various pressure transfer function descriptions $H(\mathbf{x}, \omega)$.

2.1. Case 1: $H(\mathbf{x}, \omega) = 1$

In this case the pressure is taken to be uniform over the structure, as assumed by Miles [11] and adopted in the ESDU data sheets [1]. The spectrum of the generalized force, Eq. (8), can be written in the form

$$S_{FF}(\omega) = \omega_n^2 w_{stat}^2 S_{pp}(\omega), \tag{10}$$

where

$$w_{stat} = (1/\omega_n^2) \int_{A_0} \phi_n(\mathbf{x})\, \mathrm{d}\mathbf{x}. \tag{11}$$

Here w_{stat} is the static displacement of the system under a uniform pressure loading of unit intensity. Eq. (9) then becomes

$$\sigma_w^2 = \frac{\pi \omega_n S_{pp}(\omega_n)}{4\zeta_n} w_{stat}^2, \tag{12}$$

which agrees with the established literature [11,2]. The mean squared strain at any point in the system then follows:

$$\sigma_\varepsilon^2 = \frac{\pi f_n S_{pp}(f_n)}{4\zeta_n} \varepsilon_{stat}^2, \tag{13}$$

where ε_{stat} is the static strain at that point caused by a unit pressure load, and the radian frequency ω_n has been re-expressed in Hz, f_n. It can be noted that the strain ε_{stat} can also be written in the form

$$\varepsilon_{stat} = \frac{\bar{\varepsilon}}{4\pi^2 f_n^2} \int_{A_0} \phi_n(\mathbf{x})\, \mathrm{d}\mathbf{x}, \tag{14}$$

where $\bar{\varepsilon}$ is the strain at the point of interest associated with a deflection in the form of the mode shape $\phi_n(\mathbf{x})$.

2.2. Case 2: $H(\mathbf{x}, \omega) = \phi_n(\mathbf{x})$

This is a form of "worst case" in which the pressure distribution is perfectly matched to the mode shape. Assuming that the mass per unit area m is constant over the system, Eqs. (2) and (8) yield

$$S_{FF}(\omega) = \left| \int_{A_0} \phi_n^2(\mathbf{x})\, \mathrm{d}\mathbf{x} \right|^2 S_{pp}(\omega) = S_{pp}(\omega)/m^2. \tag{15}$$

In this case Eq. (9) becomes

$$\sigma_w^2 = \frac{S_{pp}(f_n)}{64\pi^3\zeta_n f_n^3 m^2}. \tag{16}$$

Now $S_{pp}(\omega)$ is the spectrum of the reference pressure, $p(t)$ say, defined in the present case ($H = \phi_n$) such that the pressure at location $\mathbf{x}$ is given by $p(\mathbf{x}, t) = \phi_n(\mathbf{x})p(t)$. The spatial average of the pressure spectrum over the surface of the system is thus given by $\langle S_{pp}(\mathbf{x}, \omega)\rangle_{\mathbf{x}} = (1/mA)S_{pp}(\omega)$, where A is the surface area. Eq. (16) can therefore be written in the alternative form

$$\sigma_w^2 = \frac{\langle S_{pp}(\mathbf{x}, f_n)\rangle_{\mathbf{x}}}{64\pi^3\zeta_n f_n^3}\left(\frac{A}{m}\right). \tag{17}$$

Similarly, the mean squared strain at a particular point can be written as

$$\sigma_\varepsilon^2 = \frac{\langle S_{pp}(\mathbf{x}, f_n)\rangle_{\mathbf{x}}}{64\pi^3\zeta_n f_n^3}\left(\frac{A}{m}\right)\bar{\varepsilon}^2, \tag{18}$$

where $\bar{\varepsilon}$ is the strain at the point of interest associated with the mode shape $\phi_n(\mathbf{x})$, as defined previously.

2.3. Case 3: general $H(\mathbf{x}, \omega)$

In general, the spectrum of the pressure at the location $\mathbf{x}$ can be written in the form $S_{pp}(\mathbf{x}, f) = |H(\mathbf{x}, f)|^2 S_{pp}(f)$, where $S_{pp}(f)$ is the spectrum of the reference pressure. It then follows that the space average of the pressure spectrum is given by

$$\langle S_{pp}(\mathbf{x}, f)\rangle_{\mathbf{x}} = \frac{S_{pp}(f)}{A}\int_{A_0} |H(\mathbf{x}, f)|^2 \, \mathrm{d}\mathbf{x} \tag{19}$$

Eqs. (8), (9), and (19) then lead to the results

$$\sigma_w^2 = \frac{\langle S_{pp}(\mathbf{x}, f_n)\rangle_{\mathbf{x}}}{64\pi^3\zeta_n f_n^3}\left(\frac{A}{m}\right)J_n^2 \tag{20}$$

and

$$\sigma_\varepsilon^2 = \frac{\langle S_{pp}(\mathbf{x}, f_n)\rangle_{\mathbf{x}}}{64\pi^3\zeta_n f_n^3}\left(\frac{A}{m}\right)\bar{\varepsilon}^2 J_n^2, \tag{21}$$

where

$$J_n^2 = \frac{|\int_{A_0} H(\mathbf{x}, f)\phi_n(\mathbf{x}) \, \mathrm{d}\mathbf{x}|^2}{\int_{A_0} |H(\mathbf{x}, f)|^2 \, \mathrm{d}\mathbf{x} \int_{A_0} \phi_n^2 \, \mathrm{d}\mathbf{x}}. \tag{22}$$

The term J_n^2 is a form of "joint acceptance" between the mode shape and the pressure distribution. The maximum value of J_n^2 occurs for Case 2 ($H(\mathbf{x}, f) = \phi_n$) where $J_n^2 = 1$.

2.4. Estimation of the r.m.s. strain response using the single-degree-of-freedom approximation

In order to estimate the r.m.s. strain response of the four test panels using the s.d.o.f. approximations developed previously, calculation of the mode shapes and natural frequencies of

vibration is required, whilst the applied pressure spectrum at the reference point in the PWT and the viscous damping ratio are measured quantities given in Part 1 of this study [7].

2.4.1. Natural frequency of vibration, mode shapes, and modal strains

A finite element analysis was performed in order to determine the natural frequencies of vibration, the mode shapes, and associated modal strains, and the latter two quantities were normalized in accordance with the unit generalized mass matrix. This was done using the FE models developed and reported in a recent publication [8] with spring supported boundary conditions, as shown in Fig. 1 for panel 1 (the physical properties of the various panels considered here are given in Part 1 [7] and in Refs. [8,12]). The modal direct strains were recovered for each of the five inner and outer strain gauge locations. All of the modal strains were calculated for the predominant mode of vibration excited by the PWT, in this case mode 2 for panels 1–3, and mode 3 for panel 4, and are given in Table 1.

2.4.2. Reference pressure spectrum level, $S_{pp}(f_n)$ and modal damping, ζ_n

The r.m.s. acoustic pressure applied to the panels was obtained from the measurements taken using the microphone located in the aperture of the PWT, as reported in Part 1 of this study. The spectra were ensemble averaged during the FFT process, which was carried out using Welch's method [13]. Despite this averaging, the spectrum levels still appeared to contain a fair degree of noise, as can be seen in Fig. 2, which shows the levels at each OASPL for panel 1. To this end, and for the purposes of the s.d.o.f. method used in the analysis, the spectrum levels at each OASPL were averaged over the mean-square bandwidth centred on the fundamental response frequency excited by the PWT. This was carried out using the method proposed by Newland [10]. For the case of a s.d.o.f. system, the mean-square bandwidth is [10] (Fig. 3)

$$B_{\sigma^2} = \pi\zeta_n\omega_n. \tag{23}$$

The levels are then smoothed by averaging over n adjacent spectra using [10]

$$\hat{S}_{pp}(f_k) = \frac{1}{(2n+1)} \sum_{m=-n}^{n} \tilde{S}_{pp}(f_{k+m}). \tag{24}$$

Both the noisy and smoothed spectra are presented, and as can be seen there is a certain degree of variability in the spectrum levels, which was obviously not as apparent in the decibel plots presented in Part 1 of this study due to the logarithmic scale. This variability will introduce a certain amount of uncertainty in the predicted response, and to this end the standard deviation in the smoothed spectrum level over the mean-square bandwidth is presented along with the average spectrum levels in Table 2 so that a feel for the degree of uncertainty in the results can be obtained. The near regular spacing of the smoothed peaks in Fig. 2 suggests that the variability in the spectrum level arises from acoustic reflections from the first bend in the PWT duct downstream of the test aperture.

The final value needed for the s.d.o.f. calculations is the modal damping for the predominant mode excited by the PWT, which was obtained from the experimental measurements using the half-power point method. The damping values for each panel are given in Part 1 [7] in the form of equivalent viscous damping ratios.

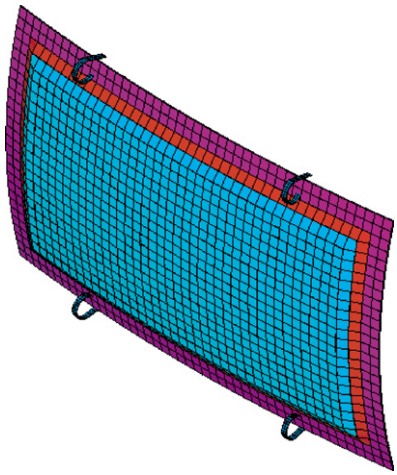

(a) FE model of panel 1

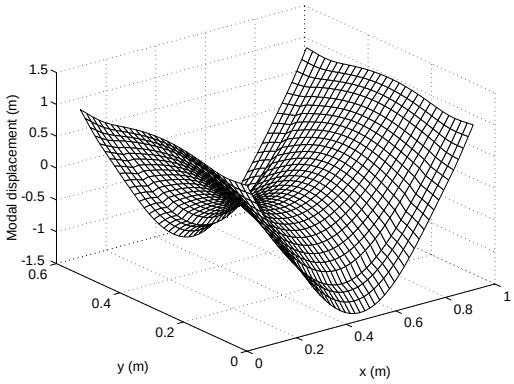

(b) Panel 1 modal displacement

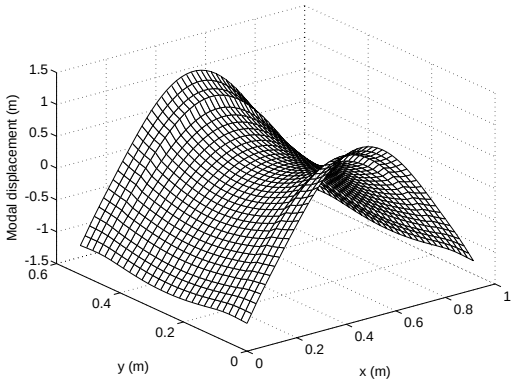

(c) Panel 2 modal displacement

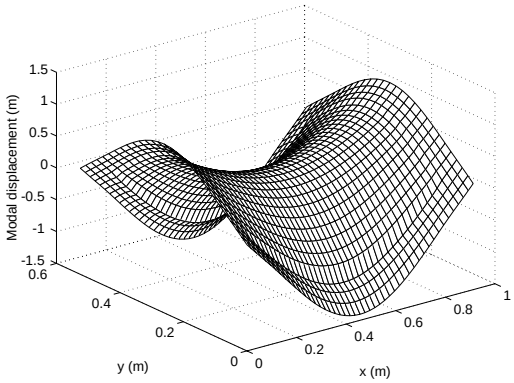

(d) Panel 3 modal displacement

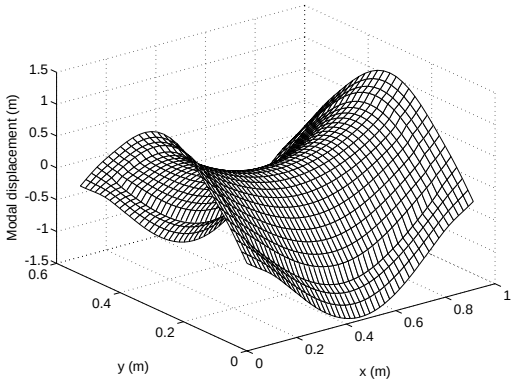

(e) Panel 4 modal displacement

Fig. 1. FE model of panel 1, and calculated modal displacement associated with the fundamental frequency of vibration excited by the PWT for the four test panels: (a) FE Model of panel 1; (b) panel 1 modal displacement; (c) panel 2 modal displacement; (d) panel 3 modal displacement; and (e) panel 4 modal displacement.

Table 1
Calculated (FE) modal strains for each strain gauge location and for each test panel (the modal strains have been normalized with respect to unit generalized mass in the FE calculations)

Panel	Modal strain ($\varepsilon \times 10^3$)									
	gi1	gi2	gi3	gi4	gi5	go1	go2	go3	go4	go5
1	126.6	221.7	233.4	87.4	84.1	287.9	171.3	176.3	294.9	284.1
2	162.9	163.3	168.8	164.0	160.0	237.2	130.9	131.2	204.2	198.3
3	53.0	312.3	349.6	64.1	63.5	199.0	257.4	278.8	144.9	140.3
4	86.6	446.7	501.7	93.1	93.3	155.3	160.8	176.1	101.5	98.7

Details of the gauge locations are given in Ref. [7].

2.4.3. Comparison of experimental and theoretical results for r.m.s. strain

In order to compare the estimated results for r.m.s. strain with the experimental results it was necessary to adjust the latter since the s.d.o.f. calculations are based around the resonant response frequency of interest while the experimental measurements were an overall r.m.s. value over a 1000 Hz bandwidth. The mean-square bandwidth of the approximation method is obviously much smaller than the response bandwidth of the experiments, and therefore in order to scale the experimental results, the percentage contribution of the predominant mode excited by the PWT to the overall response was used as the scaling factor. This was obtained from the plots of the normalized integral across the strain power spectral density, examples of which can be found in Part 1 of this study. The resulting narrowband scaling factors for each of the strain gauges and for each panel are given in Table 3.

For Case 1, the integral of the mode shapes (required in Eq. (11)) were found to be 3.70×10^{-3}, 3.80×10^{-3}, 1.70×10^{-3}, and $8.20 \times 10^{-3}\,\mathrm{m^2/kg^{1/2}}$ for panels 1–4, respectively. Using Eq. (13) together with the calculated (FE) modal strains given in Table 1 and the natural frequency of vibration, the narrowband pressure spectrum levels given in Table 2, and the previously measured damping value for the fundamental mode, the estimates for the strain response were calculated, and are presented in Table 4. The results are significantly lower than the measured strains which are given in Table 5, even after the latter have been scaled to account for the estimated response being centred on the fundamental response resonance frequency of the first bending mode. The reason for the very low theoretical prediction can be traced to the fact that the panel is located in the PWT aperture by using circular steel springs. This arrangement leads to a fundamental mode that is almost a rigid-body translation, and which therefore has almost the same spatial distribution as a uniform pressure load. This mode is orthogonal to all the higher modes of the panel, and thus the integral of a higher mode shape multiplied by a constant will be almost zero, i.e., the integral that appears in Eq. (11) will be very small. Thus a uniform pressure load produces almost no excitation of the mode selected for the theoretical prediction (the first bending mode, based on the experimental results of Part 1 [7]), and a very small strain is predicted. The problem with the prediction is not that the wrong mode has been selected, but rather that the actual pressure loading is very different from a uniform distribution, as discussed in what follows.

The theoretical results for Case 2, where the spatial distribution of the pressure loading is assumed to exactly match the mode shape, are given in Table 6. As can be seen, this assumption

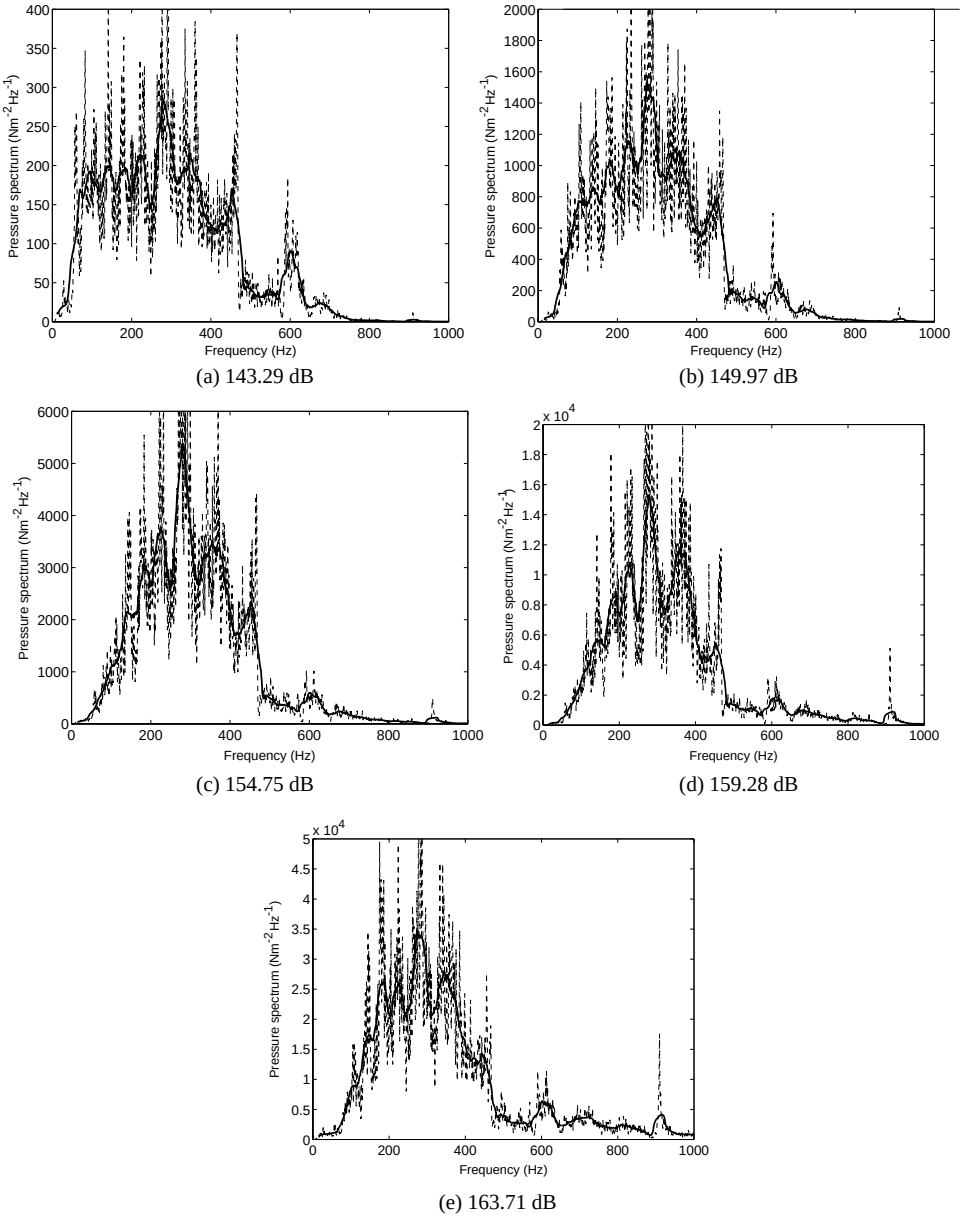

(a) 143.29 dB (b) 149.97 dB

(c) 154.75 dB (d) 159.28 dB

(e) 163.71 dB

Fig. 2. Spectrum levels of acoustic pressure for panel 1 tests and for each OASPL. Original spectrum (–), smoothed spectrum (thick line) with $n = 20$ (see Eq. (24)): (a) 143.29 dB; (b) 149.97 dB; (c) 154.75 dB; (d) 159.28 dB; and (e) 163.71 dB.

leads to an overestimate of the response compared with the scaled measured strains given in Table 4. This is understandable since the assumption that the spatial distribution of the pressure load exactly matches the mode shape of the panel is unlikely in practice. This assumption was

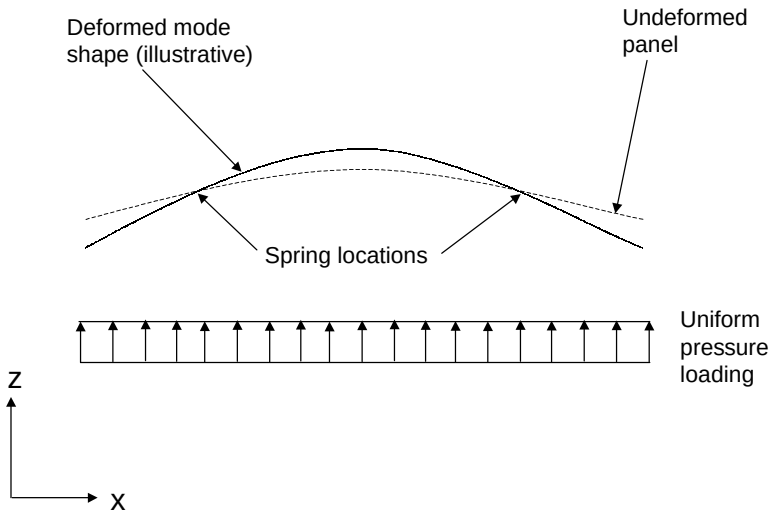

Fig. 3. Illustration of the uniform pressure loading (Case 1 assumption) and resulting fundamental mode of response of the doubly curved test panels located in the PWT.

Table 2
OASPL and associated single-sided broadband pressure spectrum levels for the four panel tests in the PWT

Panel	OASPL (dB)	$\bar{S}_{pp}(f_n)$ (Pa^2/Hz)	Standard deviation (Pa^2/Hz)
1	143.29	174.9	9.2
	149.97	869.8	18.7
	154.75	2839.5	106.8
	159.28	7448.6	396.7
	163.71	21230.0	471.3
2	143.88	138.6	7.6
	149.91	492.8	98.9
	154.92	1484.9	170.4
	159.00	3488.7	345.5
	163.09	9776.6	983.4
3	143.51	183.1	23.7
	149.93	774.2	160.8
	154.18	2535.9	474.6
	158.84	6661.0	821.5
	162.82	17614.0	1615.4
4	143.20	271.3	11.3
	149.49	1340.1	30.0
	154.69	4426.6	122.8
	159.49	12472.0	525.8
	163.71	29374.0	2551.2

Table 3
Narrowband scaling factors applied to the experimental r.m.s. strain measurements

Panel	OASPL	Narrowband scaling factor									
	(dB)	gi1	gi2	gi3	gi4	gi5	go1	go2	go3	go4	go5
1	143.29	0.88	0.88	0.84	0.85	0.80	0.93	0.77	0.75	0.87	0.88
	149.97	0.89	0.88	0.85	0.86	0.82	0.94	0.80	0.77	0.87	0.88
	154.75	0.90	0.90	0.87	0.87	0.84	0.94	0.83	0.80	0.90	0.90
	159.28	0.90	0.90	0.87	0.87	0.85	0.94	0.83	0.80	0.90	0.90
	163.71	0.93	0.92	0.90	0.91	0.89	0.96	0.87	0.85	0.93	0.93
2	143.88	0.86	0.91	0.91	0.90	0.85	0.91	0.91	0.89	0.94	0.93
	149.91	0.88	0.91	0.91	0.90	0.83	0.91	0.92	0.90	0.94	0.92
	154.92	0.83	0.87	0.87	0.86	0.79	0.88	0.89	0.87	0.92	0.88
	159.00	0.85	0.89	0.89	0.88	0.79	0.89	0.91	0.89	0.93	0.89
	163.09	0.88	0.91	0.91	0.89	0.82	0.90	0.93	0.91	0.94	0.91
3	143.51	0.80	0.82	0.81	0.25	0.27	0.82	0.79	0.80	0.33	0.43
	149.93	0.74	0.82	0.81	0.23	0.25	0.83	0.79	0.81	0.33	0.38
	154.18	0.76	0.85	0.84	0.26	0.28	0.86	0.83	0.84	0.38	0.41
	158.84	0.76	0.86	0.85	0.27	0.28	0.87	0.83	0.85	0.41	0.43
	162.82	0.78	0.88	0.88	0.33	0.32	0.89	0.86	0.88	0.48	0.49
4	143.20	0.77	0.69	0.72	0.61	0.78	0.72	0.54	0.55	0.09	0.24
	149.49	0.75	0.74	0.77	0.66	0.81	0.77	0.59	0.62	0.11	0.16
	154.69	0.77	0.79	0.81	0.70	0.85	0.81	0.64	0.66	0.14	0.18
	159.49	0.80	0.82	0.83	0.74	0.87	0.85	0.68	0.70	0.18	0.21
	163.71	0.82	0.84	0.84	0.76	0.89	0.87	0.70	0.72	0.19	0.23

investigated further by Blevins [6], and will be covered in the next section. It can be seen that Cases 1 and 2 provide the lower and upper bounds on the response, hence a more accurate estimation of the nature of the applied loading will be required in order the arrive at an improved estimate.

The joint acceptance for a general loading distribution was defined previously (see Eq. (22)). In order to arrive at an improved prediction of the dynamic strain response, a realistic estimate of the spatial distribution of the pressure must be provided. Since the test panels were located in a PWT, the excitation can be considered to be travelling acoustic waves at grazing incidence. Assuming that the waves are uni-directional, travelling along the axis of the duct, the spatial distribution of the pressure loading can be written in the form

$$H(x_1,f) = \mathrm{e}^{-\mathrm{i}k_a x_1}, \tag{25}$$

where $k_a = \omega_n/c$ is the acoustic wavenumber, ω_n is the natural frequency of vibration of the relevant mode of the test panel ($\omega_n = 2pif_n$), and c is the speed of sound which is approximately 343 m/s at sea level with standard atmospheric conditions, and x_1 is the position along the long side dimension of the panel. Eq. (25) arises from the Fourier transform of a travelling wave pressure field of the form $p(x_1,t) = p(0,t - x_1/c)$. A rapid estimate of the joint acceptance can be obtained by using the results for the mode shape from the FE modal analysis. By summing the

Table 4
Estimated r.m.s. strain for the 10 strain gauges located on the four test panels. Single-degree-of-freedom approximation method (Case 1—uniform pressure loading assumption)

Panel	f_n	ζ_n	$\int\{\phi_n\}_i \, dA$	$S_{pp}(f)$	Estimated r.m.s. strain ($\mu\varepsilon$)									
	(Hz)		($m^2/kg^{1/2}$)	(Pa^2/Hz)	gi1	gi2	gi3	gi4	gi5	go1	go2	go3	go4	go5
1	219.02	0.0105	3.70e–3	174.9	0.42	0.73	0.77	0.29	0.28	0.95	0.57	0.58	0.98	0.94
				869.8	0.93	1.64	1.72	0.65	0.62	2.12	1.26	1.30	2.18	2.10
				2839.5	1.69	2.95	3.11	1.17	1.12	3.84	2.28	2.35	3.93	3.79
				7448.6	2.73	4.79	5.04	1.89	1.82	6.21	3.70	3.81	6.36	6.13
				21230	4.61	8.08	8.50	3.19	3.06	10.49	6.24	6.43	10.75	10.35
2	164.30	0.0120	3.80e–3	138.6	0.71	0.71	0.74	0.71	0.70	1.04	0.57	0.57	0.89	0.86
				492.8	1.34	1.34	1.39	1.35	1.31	1.95	1.07	1.08	1.68	1.63
				1484.9	2.32	2.33	2.40	2.34	2.28	3.38	1.87	1.87	2.91	2.83
				3488.7	3.56	3.57	3.69	3.58	3.50	5.18	2.86	2.87	4.46	4.33
				9776.6	5.95	5.97	6.17	5.99	5.85	8.67	4.79	4.80	7.47	7.25
3	272.62	0.0125	1.70e–3	183.1	0.05	0.32	0.36	0.07	0.07	0.20	0.26	0.29	0.15	0.14
				774.2	0.11	0.66	0.74	0.14	0.13	0.42	0.54	0.59	0.31	0.30
				2535.9	0.20	1.19	1.34	0.25	0.24	0.76	0.98	1.06	0.55	0.54
				6661.0	0.33	1.93	2.16	0.40	0.39	1.23	1.59	1.73	0.90	0.87
				17614	0.53	3.14	3.52	0.65	0.64	2.00	2.59	2.81	1.46	1.41
4	288.67	0.0102	8.20e–3	271.3	0.53	2.73	3.07	0.57	0.57	0.95	0.98	1.08	0.62	0.61
				1340.1	1.18	6.08	6.82	1.27	1.27	2.11	2.19	2.40	1.38	1.34
				4426.6	2.14	11.04	12.40	2.30	2.31	3.84	3.98	4.35	2.51	2.44
				12472	3.59	18.54	20.82	3.87	3.87	6.45	6.67	7.31	4.21	4.10
				29374	5.51	28.45	31.95	5.93	5.94	9.89	10.24	11.21	6.47	6.29

modal displacemements for the mode shape in question, and multiplying by the area of the panel divided by the number of nodes, an estimate of the integral of the mode shape is obtained. The expression for the joint acceptance (Eq. (22)) therefore becomes

$$J_n^2 = \frac{|\sum_{j=1}^{N} \phi_j e^{-ik_a x_j}|^2}{\sum_{j=1}^{N} |e^{-ik_a x_j}|^2 \sum_{j=1}^{N} \phi_j^2}, \tag{26}$$

where ϕ_j is the modal displacement at each node j for the mode shape in question, x_j is the nodal co-ordinate in the x direction (along the long side of the panel) for each node j, and N is the number of nodes in the FE model.

The r.m.s. strain results for Case 3, obtained by employing Eq. (26), are given in Table 7. A comparison is made with the measured r.m.s. strains, which have been scaled according to the percentage contribution of the fundamental mode response to the overall r.m.s. measured strains, using the scale factors given in Table 3. The comparison for each panel is shown in Figs. 4 and 5. The results show excellent agreement between measured and predicted values, with the majority of the results falling within a $\pm 30\%$ confidence band. This is a very favourable result when one

Table 5
Measured r.m.s. strain for the 10 strain gauges located on the four test panels

Panel	$S_{pp}(f)$	Measured r.m.s. strain (scaled) ($\mu\varepsilon$)									
	(Pa^2/Hz)	gi1	gi2	gi3	gi4	gi5	go1	go2	go3	go4	go5
	174.9	7.9	10.5	10.7	5.7	4.5	14.7	7.6	8.3	14.4	12.9
	869.8	16.2	23.4	24.1	11.6	8.9	32.4	16.9	18.5	31.9	27.5
1	2839.5	28.7	42.0	43.8	19.4	15.9	57.9	30.9	33.8	58.2	49.8
	7448.6	49.7	72.6	75.5	31.7	27.7	101.2	53.2	58.2	100.9	86.2
	21230	92.9	134.3	139.9	60.7	52.9	189.1	99.1	108.7	189.1	161.4
	138.6	6.4	7.7	7.3	6.0	6.0	9.3	6.6	5.6	8.5	8.6
	492.8	11.5	15.3	14.4	11.5	11.1	18.6	13.1	11.0	16.9	15.5
2	1484.9	17.3	23.8	22.4	17.8	17.0	29.0	20.8	17.6	26.4	23.6
	3488.7	30.0	41.5	39.1	31.0	29.3	50.6	36.9	31.2	45.9	40.6
	9776.6	51.9	71.5	67.2	53.3	51.2	87.1	64.0	54.8	78.6	69.8
	183.1	4.0	9.2	9.5	1.2	1.3	7.2	7.8	8.4	3.5	4.6
	774.2	5.9	19.4	20.1	2.1	2.2	15.4	16.9	18.3	7.4	7.9
3	2535.9	9.5	35.0	36.4	3.8	4.0	27.1	30.3	33.1	13.6	13.8
	6661.0	15.8	60.5	63.0	6.6	6.7	47.7	51.4	56.6	25.1	24.2
	17614	27.2	107.4	111.0	12.8	12.2	82.7	89.2	98.5	48.3	45.3
	271.3	4.5	10.5	13.1	2.5	3.8	4.2	3.9	4.1	0.9	2.4
	1340.1	8.0	26.9	33.5	5.6	8.0	9.7	9.7	10.5	2.3	3.3
4	4426.6	14.9	55.1	67.5	11.0	15.8	19.6	19.6	21.4	5.4	6.3
	12472	28.6	110.4	132.6	20.9	30.8	39.0	38.4	41.8	11.7	12.9
	29374	47.8	182.7	215.7	34.5	50.6	65.4	63.4	69.0	19.9	22.1

Scaled using narrowband scaling factors given in Table 3.

considers that the current design guidelines are reported to give results within a factor of 2 compared with measured data [5].

Finally, the outer-to-inner r.m.s. predicted strain ratios are given in Table 8, for comparison with the measured ratios presented in Part 1. The predicted ratios were found to remain constant with increasing OASPL. The ratios for gauges 2 and 3 compare very well with the average measured ratios for panels 1, 2, and 3, whereas for panel 4 the predicted ratio is slightly lower compared with the measured ratio. Gauges 4 and 5 show similar results except for panel 1 which shows a higher predicted ratio compared with the measured ratio.

3. Application of Blevins' normal mode method

A modification of the classical Miles [11] equation has been proposed by Blevins [6]. In this study, the spatial characteristics of both the structural modes and the sound field were considered simultaneously and related in order to arrive at a method that extended the Miles approach to higher modes and complex shapes. In general, for a linear elastic plate or shell structure excited by

Table 6
Estimated r.m.s. strain for the 10 strain gauges located on the four test panels. Single-degree-of-freedom approximation method (Case 2—unit joint acceptance assumption)

Panel	$S_{pp}(f)$	Estimated r.m.s. strain ($\mu\varepsilon$)									
	(Pa^2/Hz)	gi1	gi2	gi3	gi4	gi5	go1	go2	go3	go4	go5
	174.9	33.95	59.44	62.57	23.44	22.54	77.18	45.93	47.28	79.06	76.17
	869.8	75.71	132.54	139.52	52.28	50.27	172.11	102.43	105.43	176.30	169.85
1	2839.5	136.78	239.48	252.09	94.46	90.82	310.98	185.07	190.49	318.55	306.89
	7448.6	221.54	387.87	408.30	152.99	147.10	503.67	299.74	308.52	515.93	497.06
	21230	374.02	654.82	689.31	258.28	248.34	850.32	506.04	520.86	871.02	839.16
	138.6	55.30	55.46	57.29	55.70	54.34	80.54	44.45	44.55	69.32	67.35
	492.8	104.27	104.57	108.03	105.02	102.47	151.87	83.81	84.00	130.72	126.99
2	1484.9	180.99	181.52	187.53	182.30	177.87	263.62	145.48	145.82	223.92	220.44
	3488.7	277.43	278.22	287.45	279.43	272.65	404.08	222.99	223.51	347.81	337.89
	9776.6	464.42	465.75	481.20	467.78	456.42	676.44	373.30	374.16	582.25	565.63
	183.1	9.40	55.41	62.04	11.37	11.27	35.32	45.68	49.46	25.70	24.90
	774.2	19.33	113.94	127.57	23.37	23.18	72.62	93.93	101.71	52.86	51.21
3	2535.9	34.98	206.21	230.88	42.30	41.95	131.43	169.99	184.08	95.66	92.67
	6661.0	56.69	334.20	374.19	68.56	67.99	213.00	275.51	298.33	155.04	150.20
	17614	92.19	543.46	608.49	111.49	110.57	346.38	448.01	485.13	252.12	244.24
	271.3	19.00	98.02	110.09	20.44	20.47	34.08	35.28	38.64	22.27	21.66
	1340.1	42.23	217.85	244.67	45.43	45.50	75.75	78.43	85.87	49.50	48.15
4	4426.6	76.75	395.93	444.67	82.56	82.70	137.68	142.55	156.07	89.97	87.51
	12472	128.82	664.59	746.40	138.59	138.81	231.10	239.27	261.96	151.02	146.89
	29374	197.70	1019.93	1145.48	212.68	213.03	354.66	367.20	402.03	231.77	225.43

an acoustic pressure over the entire surface, the response of each mode is given by [6]

$$(1/\omega_n^2)\ddot{w}_n(t) + (2\zeta_n/\omega_n)\dot{w}_n(t) + w_n(t) = Jp(t), \tag{27}$$

where

$$J = \frac{\int \tilde{p}_n(\mathbf{x})\tilde{w}_n(\mathbf{x})\,\mathrm{d}\mathbf{x}}{\omega_n^2 \int m\tilde{w}_n^2(\mathbf{x})\,\mathrm{d}\mathbf{x}} \tag{28}$$

is the modal joint acceptance which is constant for each mode. The equations have been written in the notation used by Blevins, where $\tilde{p}_n$ defines the spatial characteristics of the pressure field (equivalent to $H(\mathbf{x},f)$ which is used in the present work), $\tilde{w}_n$ is the response mode shape, and the other symbols have their usual meanings. As can be seen, the time and spatial dependence of the response have been separated, which allowed solutions to be generated independently and later assembled to give the complete solution [6]. The remainder of the study [6] concentrated on the approximation of the joint acceptance, J. Blevins noted that for aircraft applications where, generally, the acoustic pressure load has a very rich frequency content and complex distribution, the determination of J by means such as estimation from historical data, measurement from a

Table 7
Estimated r.m.s. strain for the 10 strain gauges located on the four test panels. Single-degree-of-freedom approximation method (Case 3—estimated joint acceptance assumption)

Panel	$S_{pp}(f)$	Estimated r.m.s. strain ($\mu\varepsilon$)									
	(Pa^2/Hz)	gi1	gi2	gi3	gi4	gi5	go1	go2	go3	go4	go5
	174.9	8.94	15.65	16.47	6.17	5.94	20.32	12.09	12.45	20.82	20.05
	869.8	19.93	34.90	36.74	13.77	13.24	45.32	26.97	27.76	46.42	44.72
1	2839.8	36.02	63.06	66.38	24.87	23.91	81.88	48.73	50.16	83.87	80.81
	7448.6	58.33	102.13	107.50	40.28	38.73	132.62	78.92	81.23	135.84	130.88
	21230	98.48	172.42	181.50	68.01	65.39	223.89	133.24	137.14	229.34	220.95
	138.6	9.99	10.02	10.35	10.06	9.82	14.55	8.03	8.05	12.52	12.17
	492.8	18.84	18.89	19.52	18.97	18.51	27.44	15.14	15.17	23.61	22.94
2	1484.9	32.70	32.79	33.88	32.93	32.13	47.62	26.28	26.34	40.99	39.82
	3488.7	50.12	50.26	51.93	50.48	49.25	72.99	40.28	40.38	62.83	61.04
	9776.6	83.90	84.14	86.93	84.50	82.45	122.20	67.44	67.59	105.18	102.18
	183.1	1.70	10.00	11.19	2.05	2.03	6.37	8.24	8.92	4.64	4.49
	774.2	3.49	20.55	23.01	4.22	4.18	13.10	16.94	18.35	9.54	9.24
3	2535.9	6.31	37.20	41.65	7.63	7.57	23.71	30.67	33.21	17.26	16.72
	6661.0	10.22	60.29	67.50	12.37	12.27	38.43	49.70	53.82	27.97	27.10
	17614	16.63	98.04	109.77	20.11	19.95	62.49	80.82	87.52	45.48	44.06
	271.3	2.74	14.13	15.87	2.95	2.95	4.91	5.09	5.57	3.21	3.12
	1340.1	6.09	31.41	35.28	6.55	6.56	10.92	11.31	12.38	7.14	6.94
4	4426.6	11.07	57.09	64.12	11.91	11.93	19.85	20.56	22.50	12.97	12.62
	12472	18.58	95.83	107.63	19.98	20.02	33.32	34.50	37.77	21.78	21.18
	29374	28.51	147.07	165.18	30.67	30.72	51.14	52.95	57.97	33.42	32.51

number of microphones, or analytical prediction is by no means a simple task. This is particularly true for intake ducts where the acoustic pressure load consists of discrete tones superimposed on a broadband spectrum with a very complex spatial distribution along the duct. To this end, several approximations were suggested, such as $\tilde{p}_n(\mathbf{x}) = 1$, a constant over the surface which is basically the Miles approach. The approximation is most applicable when the acoustic half-wavelength exceeds the lateral dimensions of the panel. However, the disadvantage of this approximation is that it is incapable of showing any excitation of antisymmetric modes, hence its restriction to the fundamental mode of fully clamped plates. Other suggestions included a $Sign(\tilde{w}_n(\mathbf{x}))$ function, sinusoidal functions, and finally the mass-weighted structural mode shape. The latter involves matching a point on the surface of the panel (generally the point of maximum displacement) to the applied sound pressure level, as opposed to using a unit pressure over the entire surface. Substituting,

$$\tilde{p}_n(\mathbf{x}) = \omega_n^2 m \tilde{w}_n(\mathbf{x}) \tag{29}$$

the mass-weighted mode shape approximation, into Eq. (28) and integrating, produces a joint acceptance of $J = 1$. A crude estimation of the influence of the joint acceptance in Blevins

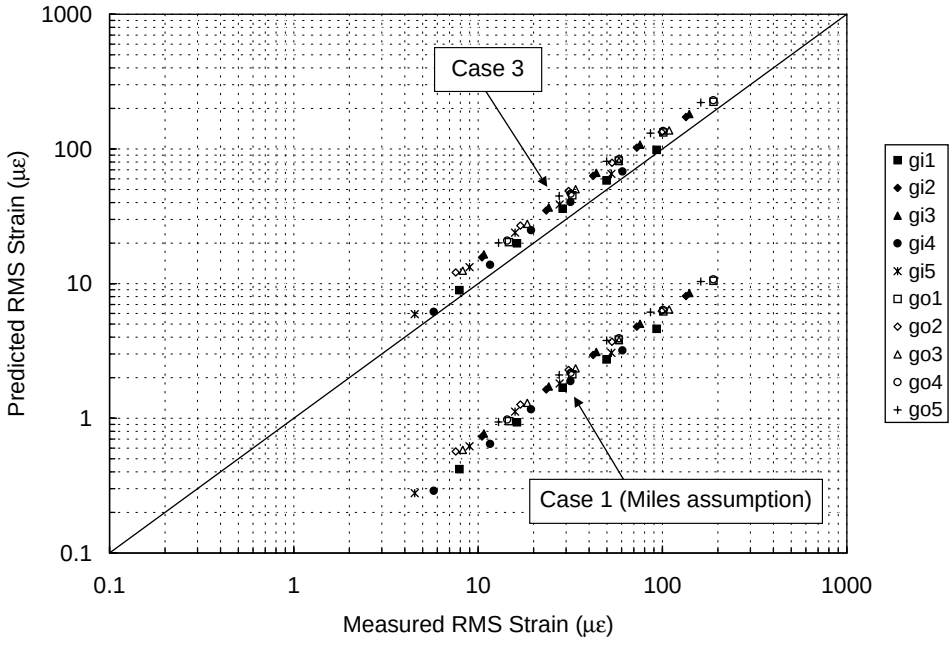

(a) Panel 1

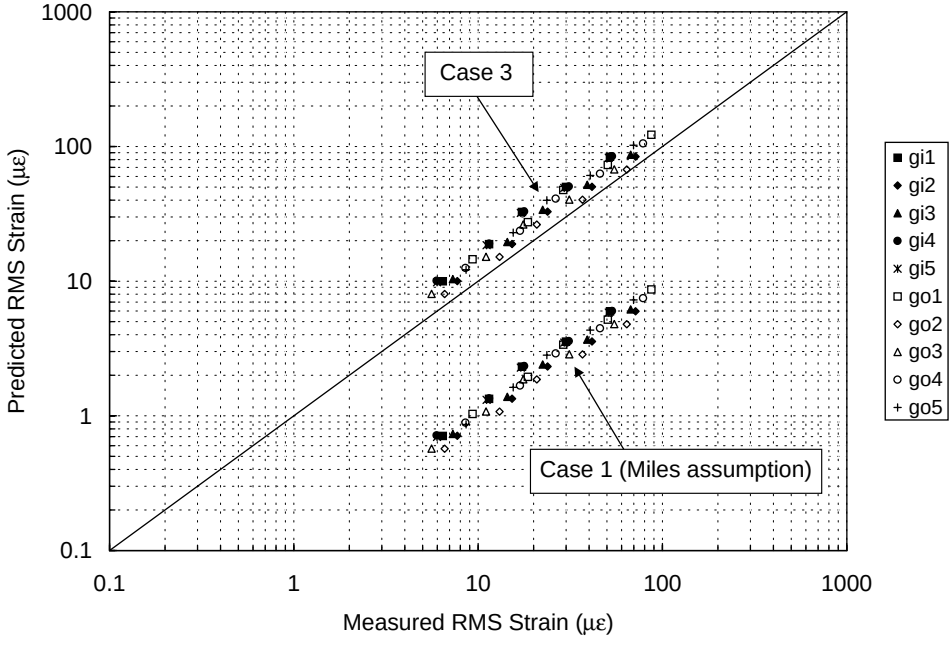

(b) Panel 2

Fig. 4. Comparison of measured and predicted (s.d.o.f. case 3 approximation method, Eqs. (21) and (26)) r.m.s. strain for panels 1 and 2. Narrowband response centred on the fundamental mode of vibration excited by the PWT. The results from the s.d.o.f. Case 1 method (Eqs. (13) and (14) —Miles approximation) have also been plotted for comparison: (a) panel 1 and (b) panel 2.

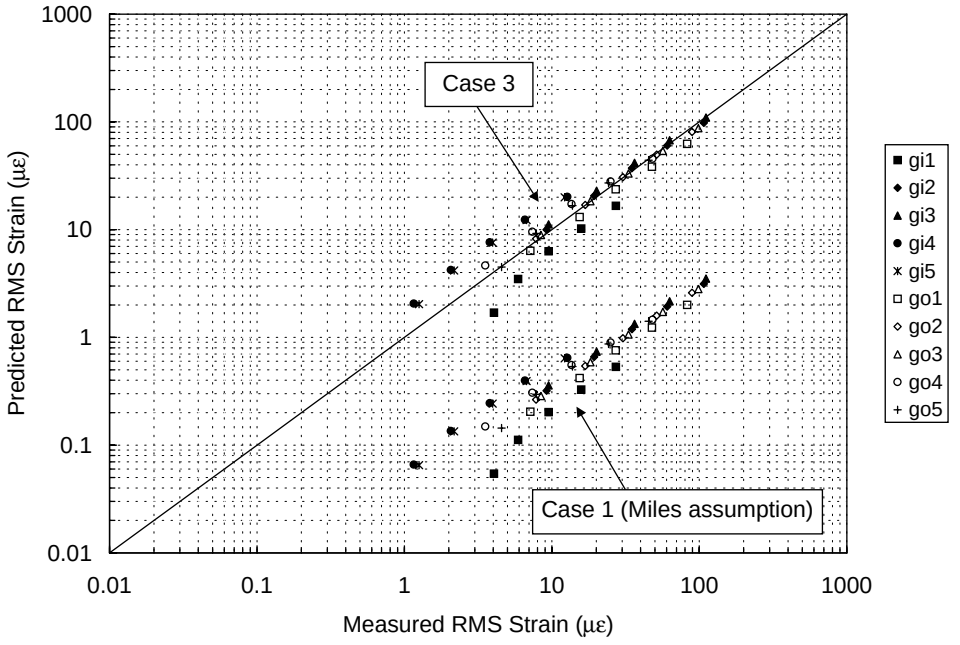

(a) Panel 3

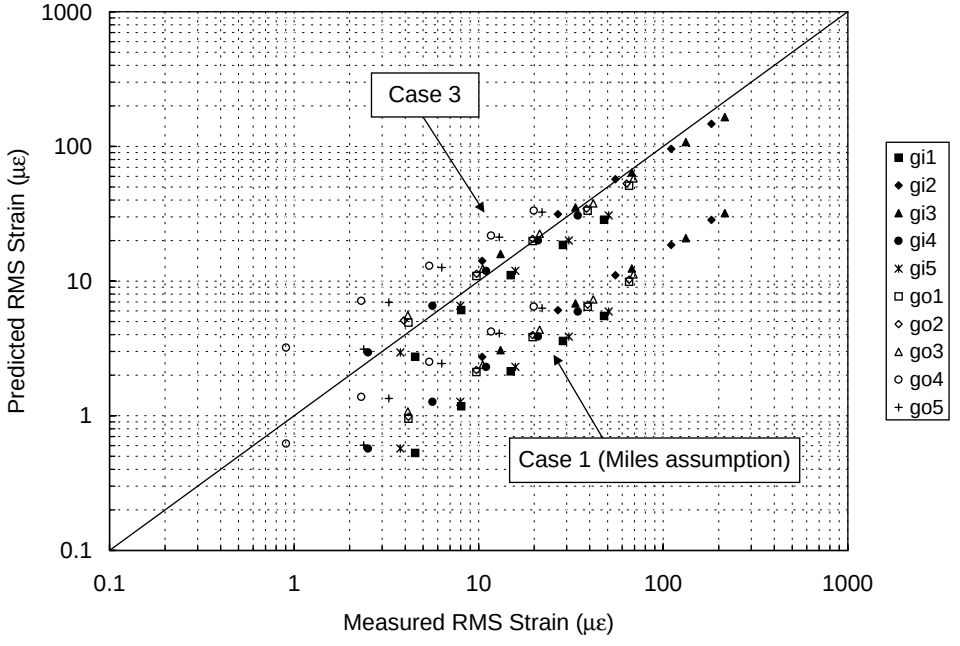

(b) Panel 4

Fig. 5. Comparison of measured and predicted (s.d.o.f. case 3 approximation method, Eqs. (21) and (26)) r.m.s. strain for panels 3 and 4. Narrowband response centred on the fundamental mode of vibration excited by the PWT. The results from the s.d.o.f. Case 1 method (Eqs. (13) and (14) —Miles approximation) have also been plotted for comparison: (a) panel 3 and (b) panel 4.

Table 8
Ratio of outer-to-inner r.m.s. strain for the predicted results using the s.d.o.f. approximation method (Case 3), and the measured mean results (standard deviation values are given in brackets)

Panel	go1/gi1	go2/gi2	go3/gi3	go4/gi4	go5/gi5
Predicted (s.d.o.f., Case 3)					
1	2.27	0.77	0.76	3.37	3.38
2	1.46	0.80	0.78	1.24	1.24
3	3.76	0.82	0.80	2.26	2.21
4	1.79	0.36	0.35	1.09	1.06
Measured mean					
1	1.89 (0.083)	0.80 (0.013)	0.85 (0.011)	2.83 (0.262)	2.85 (0.133)
2	1.55 (0.105)	0.86 (0.011)	0.79 (0.016)	1.39 (0.015)	1.26 (0.039)
3	2.37 (0.380)	0.88 (0.017)	0.90 (0.009)	2.50 (0.110)	2.37 (0.080)
4	1.19 (0.133)	0.44 (0.027)	0.39 (0.016)	2.39 (0.094)	1.91 (0.172)

formulation can be made by considering the acoustic wavelength in terms of the structural wavelength, i.e., if the acoustic half-wavelength is greater than the structural half-wavelength then the joint acceptance of unity is valid. When the acoustic half-wavelength is very much greater than the structural half-wavelength, the loading approaches the Miles assumption of uniform pressure over the surface of the panel; however, as the acoustic half-wavelength becomes smaller than the structural half-wavelength, the accuracy of the joint acceptance becomes more important to correctly estimate the response. Blevins' method should theoretically work best when the acoustic and structural half-wavelengths match. A comparison of the acoustic and structural half-wavelengths were obtained for the four experimental test panels by conducting a modal analysis using the FE models developed in Ref. [8] with boundary conditions similar to that used the PWT. A typical FE model of panel 1 is shown in Fig. 1(a), and the fundamental mode shape excited by the PWT, calculated in the modal analysis for all four panels, is shown in Figs. 1(b)–(d). As can be seen, it is fairly difficult to define the shape in terms of a number of structural half-wavelengths in either direction. However, an approximation can be made by taking the structural half-wavelength to be either the length of the panel or the distance between the spring supports (about which the panel appears to deform). A comparison is now made between the structural and acoustic half-wavelengths in both cases, the latter calculated using the relationship $\lambda_a = c/(2f)$, where c is the speed of sound in air (≈ 343 m/s) and f is the frequency of interest corresponding to the natural frequency of vibration of the structure. The results are presented for each of the four test panels in Table 9.

The results presented in Table 9 indicate that if the structural half-wavelength is taken to be equal to the length of the panel, the approximation method should work best for panel 1 and 2, although an accurate estimate of the joint acceptance will be more important for the former since the acoustic half-wavelength is smaller than the structural half-wavelength. The same is also true for panels 3 and 4, however the difference between the two wavelengths is greater which would suggest a less accurate estimate compared to the first two panels. If however, the structural half-wavelength is taken to be the distance between the spring supports, the better estimate should be obtained for panels 3 and 4, with the worst estimate arising for panel 2.

Table 9
Comparison of structural and acoustic half-wavelengths for the four test panels

Panel	f_n (Hz)	$\lambda_a/2$ (m)	λ_s/λ_a ($\lambda_s = 0.912$ m)	λ_s/λ_a ($\lambda_s = 0.505$ m)	J_{1D} (Blevins, $\lambda_s = 0.912$ m)	J_{1D} (Blevins, $\lambda_s = 0.505$ m)	J_n (Present, Eq. (26))
1	219.02	0.78	1.17	0.65	0.917	1.023	0.263
2	164.30	1.04	0.87	0.49	1.058	0.878	0.181
3	272.62	0.63	1.45	0.80	0.755	1.084	0.180
4	288.67	0.59	1.54	0.86	0.704	1.086	0.144

3.1. Approximation procedure

For broadband random acoustic excitation, where the bandwidth of excitation is greater than the response bandwidth of the mode of interest, the estimate of the r.m.s. strain using Blevins method is given by [6]

$$\varepsilon_{n_{r.m.s.}} = \left(\frac{\pi f_n S_{pp}(f)}{4\zeta_n}\right)^{1/2} \frac{\bar{\varepsilon}}{\tilde{P}_{nc}}. \tag{30}$$

The pressure spectrum level, $S_{pp}(f)$, and the natural frequencies of vibration, f_n, mode shapes, and modal strains, $\bar{\varepsilon}$ were obtained as discussed in the previous section, and the characteristic pressure, $\tilde{P}_{nc}$, was calculated using the formula [6]

$$\tilde{P}_{nc} = m(2\pi f_n)^2 |\tilde{w}_n(\mathbf{x}_c)|, \tag{31}$$

where m is the mass per unit area, f_n is the natural frequency of vibration in the mode of interest, and $\tilde{w}_n(\mathbf{x}_c)$ is the maximum modal displacement. All of the inputs to Eq. (31) were obtained from the FE model by conducting a modal analysis.

Blevins' method [6] with $J = 1$ is very similar to Case 2 of the present work. The only difference lies in the fact that in Ref. [6], $S_{pp}(f)$ is the pressure spectrum at the reference point on the panel—the pressure then varies away from this point in accordance with the mass weighted mode shape. In the present work the space averaged pressure spectrum plays the role of $S_{pp}(f)$, and this can lead to differences in the response predictions.

3.2. Estimation of the r.m.s. strain response using Blevins' method

All of the parameters needed to estimate the r.m.s. strain response of the doubly curved panels to random acoustic excitation using Blevins' method [6] are presented in Tables 2 and 10. The damping was obtained from the experimental results from the PWT tests, as presented in Section 5.5.2, and the mass per unit area for each panel was constant at 5.24 kg/m^2.

The predicted r.m.s. strain values using Blevin's matched mode approximation procedure (Eqs. (30) and (31)), for the 10 strain gauge locations on the four test panels, are presented in Table 11 and Figs. 6 and 7. The results over-predict the r.m.s. strain that was measured, where the latter values have been scaled according to the percentage contribution of the fundamental mode

Table 10
Parameters for the four doubly curved sandwich panels used in Blevin's method (modal strains, natural frequencies and maximum modal displacement obtained using FE model)

Panel	f_1	ζ_1	$\lvert\tilde{w}_1(x,y,z)\rvert$	$\tilde{P}_{nc}$	Modal strain ($\mu\varepsilon$)									
	(Hz)		(m)	(N m^{-2})	gi1	gi2	gi3	gi4	gi5	go1	go2	go3	go4	go5
1	219.02	0.0105	1.376	13.66e6	126.6e3	221.7e3	233.4e3	87.44e3	84.07e3	287.9e3	171.3e3	176.3e3	294.9e3	284.1e3
2	164.30	0.0120	1.405	7.850e6	162.9e3	163.3e3	168.7e3	164.0e3	160.0e3	237.2e3	130.9e3	131.2e3	204.2e3	198.3e3
3	272.62	0.0125	0.458	7.053e6	52.97e3	312.3e3	349.6e3	64.06e3	63.53e3	199.0e3	257.4e3	278.8e3	144.9e3	140.3e3
4	288.67	0.0102	0.653	11.26e6	86.6e3	446.7e3	501.7e3	93.1e3	93.3e3	155.3e3	160.8e3	176.1e3	101.5e3	98.7e3

Table 11
Estimated r.m.s. strain for the 10 strain gauges located on the four test panels. Blevin's approximation method

Panel	$S_{pp}(f)$	Estimated r.m.s. strain ($\mu\varepsilon$)									
	(Pa^2/Hz)	gi1	gi2	gi3	gi4	gi5	go1	go2	go3	go4	go5
	174.9	31.43	55.03	57.93	21.71	20.87	71.46	42.53	43.77	73.20	70.52
	869.8	70.10	122.72	129.18	48.40	46.54	159.35	94.83	97.61	163.23	157.26
1	2839.5	126.64	221.73	233.40	87.46	84.09	287.92	171.35	176.37	294.93	284.14
	7448.6	205.11	359.11	378.03	141.65	136.19	466.33	277.52	285.65	477.68	460.21
	21230	346.29	606.27	638.20	239.13	229.93	787.28	468.52	482.25	806.44	776.95
	138.6	54.47	54.62	56.43	54.86	53.53	79.33	43.78	43.88	68.28	66.33
	492.8	102.70	102.99	106.41	103.44	100.93	149.58	82.55	82.74	128.75	125.08
2	1484.9	178.27	178.78	184.71	179.56	175.20	259.66	143.29	143.62	223.50	217.12
	3488.7	273.25	274.04	283.12	275.23	268.54	398.00	219.64	220.15	342.58	332.80
	9776.6	457.43	458.74	473.95	460.74	449.54	666.26	367.68	368.53	573.48	557.12
	183.1	13.30	78.41	87.80	16.09	15.95	49.98	64.64	70.00	36.38	35.24
	774.2	27.35	161.24	180.53	33.08	32.81	102.77	132.92	143.94	74.80	72.46
3	2535.9	49.51	291.82	326.74	59.87	59.37	185.99	240.57	260.50	135.38	131.15
	6661.0	80.23	472.95	529.54	97.02	96.23	301.44	389.89	422.19	219.41	212.55
	17614	130.47	769.09	861.11	157.78	156.48	490.18	634.02	686.54	356.79	345.64
	271.3	18.88	97.38	109.36	20.31	20.34	33.86	35.06	38.38	22.13	21.52
	1340.1	41.95	216.42	243.06	45.13	45.20	75.26	77.92	85.31	49.18	47.83
4	4426.6	76.24	393.34	441.76	82.16	82.16	136.78	141.61	155.04	89.38	86.94
	12472	127.98	660.23	741.51	137.68	137.90	229.58	237.70	260.25	150.03	145.93
	29374	196.41	1013.23	1137.97	211.29	211.64	352.34	364.79	399.39	230.25	223.95

response to the overall r.m.s. response. The results using Blevins' matched mode method are very close to those obtained using Case 2, s.d.o.f. method presented in the previous section, where a joint acceptance of unity has been used in both methods.

An improved estimate of the joint acceptance has been proposed by Blevins, where the structural and acoustic waveforms were considered as sinusoids [6]. In addition, Blevins presented a two-dimensional form of the joint acceptance function, where it was assumed that the acoustic waves propagated along both co-ordinates and the modes of vibration are separable along these two co-ordinates [6]. In the present study, it is assumed that the pressure loading is in the form of travelling waves that propagate in one direction only, therefore Blevins one-dimensional joint acceptance is considered here. The results for joint acceptance, calculated using Blevins method for the one-dimensional case (Eqs. (46) and (47) in Ref. [6]) for both structural half-wavelength approximations are presented in Table 9. In addition, the joint acceptance values calculated using Eqs. (26), (25) and the modal displacement results, are also given in Table 9. The results clearly show that improvements to the predicted response are made by considering the spatial characteristics of the pressure loading and the structural response shape in more detail. The joint acceptance values calculated using the present method (Eqs. (26), (25) and the modal displacement results using the FE model) lead to good agreement between predicted and

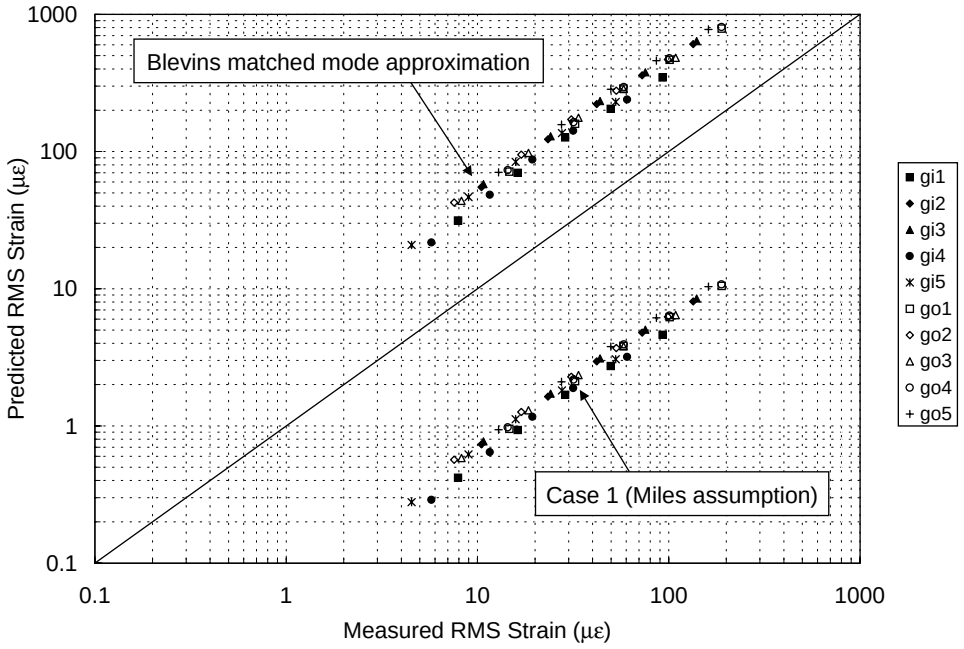

(a) Panel 1

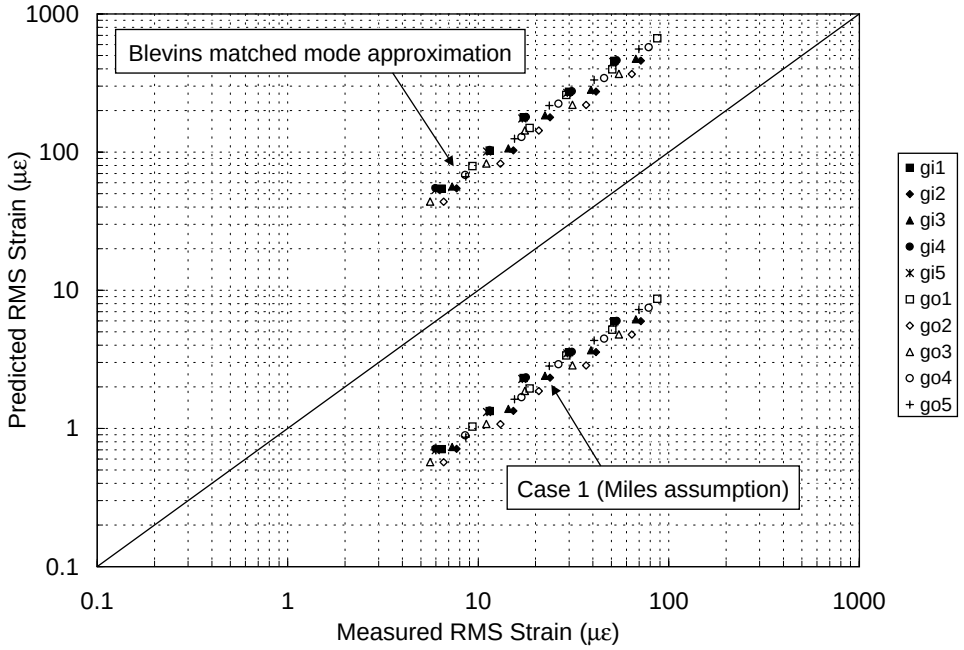

(b) Panel 2

Fig. 6. Comparison of measured and predicted r.m.s. strain for panels 1 and 2 using Blevins approximation method (matched mode shape, Eqs. (30) and (31)). Narrowband response centred on the fundamental mode of vibration excited by the PWT. The results from the s.d.o.f. Case 1 method (Eqs. (13) and (14) —Miles approximation) have also been plotted for comparison: (a) panel 1 and (b) panel 2.

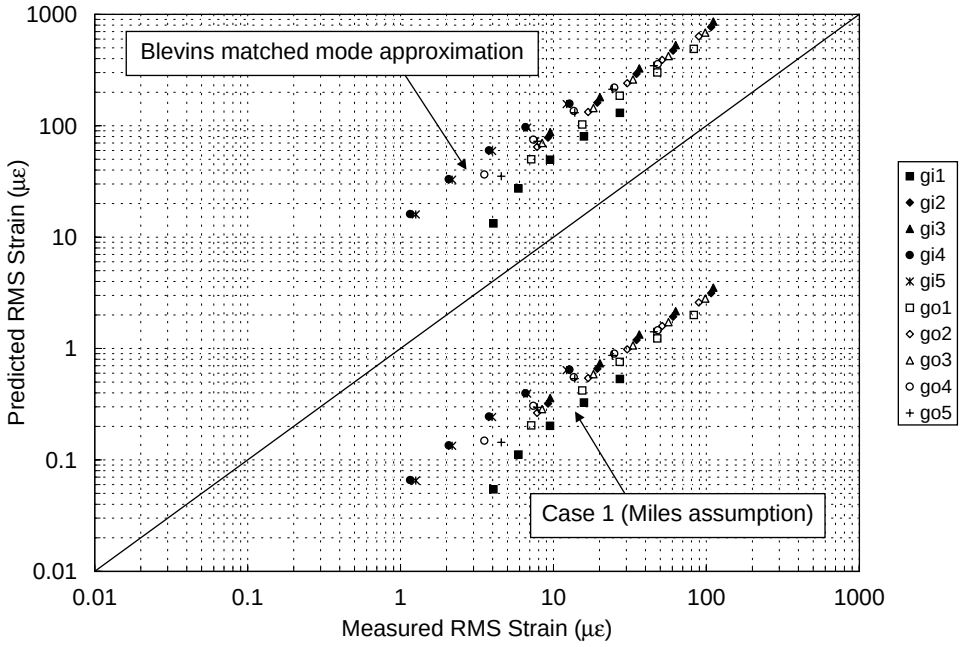

(a) Panel 3

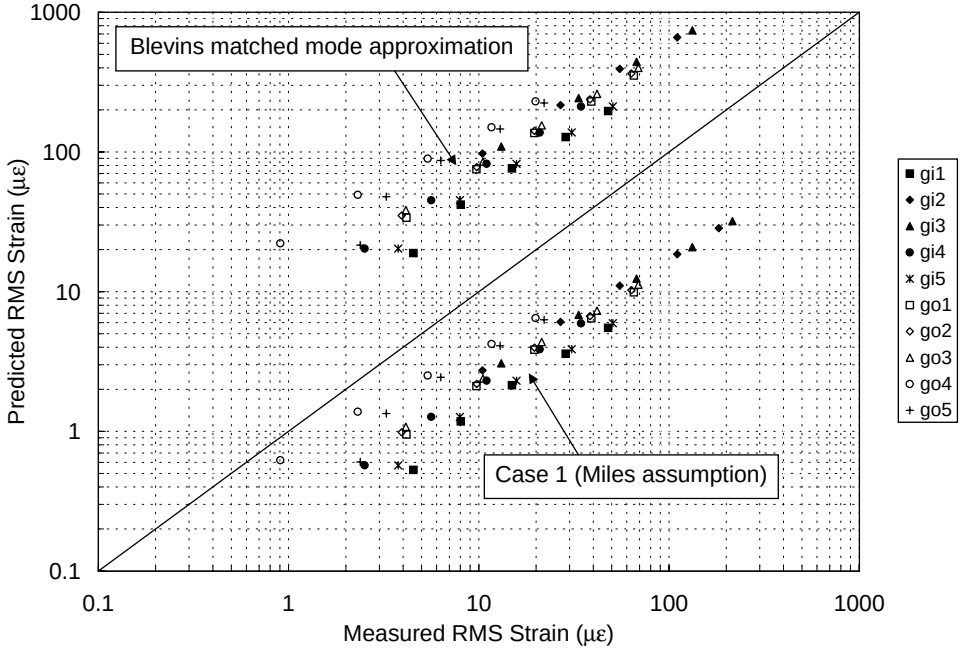

(b) Panel 4

Fig. 7. Comparison of measured and predicted r.m.s. strain for panels 3 and 4 using Blevins approximation method (matched mode shape, Eqs. (30) and (31)). Narrowband response centred on the fundamental mode of vibration excited by the PWT. The results from the s.d.o.f. Case 1 method (Eqs. (13) and (14) —Miles approximation) have also been plotted for comparison: (a) panel 3 and (b) panel 4.

measured r.m.s. strain, as demonstrated in the previous section. Using Blevins wavelength correction method, the best improvement would be made when the structural half-wavelength is taken to be equal to the length of the panel. However, for the present study where the panel boundary conditions are non-conventional, the assumption of the structural response being modelled as sinusoids cannot be used in this case. Blevins wavelength correction method was developed to avoid extensive computation of the joint acceptance [6], whereas for the present study it is necessary to compute the modal displacements using a finite element model of the structure in order to calculate the joint acceptance.

4. Dynamic response prediction using the finite element method

The ANSYS finite element models of the four test panels were used to predict the dynamic response to random acoustic excitation in the PWT. A full description of the FE models is presented in a recent publication [8], and the boundary conditions applied are discussed in Part 1 of this study [7].

Two possible options exist for modelling the random acoustic pressure loading in the PWT. The first involves dividing the structure into zones of equal surface area, in which the pressure PSD is assumed to be spatially correlated over each zone. Ideally, each zone should be the size of each finite element in the model, but this would create a huge amount of data in this case since each model contains approximately 1200 elements. It would therefore be more convenient to define larger zones, say eight in total, over the entire surface of the panel.

The second option is to model a series of travelling waves over the whole surface of the panel within the frequency range of interest, and this was the option used to generate a solution for the acoustically excited doubly curved panels located in the PWT. The analysis was divided into 10 Hz frequency bands from 47 to 545 Hz in which the acoustic wavenumber, k_1 was held constant. A harmonic analysis, using the modal superposition method, was carried out in each frequency band with five sub-step calculations made, centred on the frequency step in the loop. Within each of these frequency bands, the loading was applied in lines which ran the length of the short side, and were spaced at intervals equal to the element edge length from one end of the panel to the other along the long side. Unit forces were applied at the corner nodes on these lines, and the real and imaginary parts of the load were defined according to the x_{1_n}-location of the nodal line, and the frequency step being analysed, which along with the convection velocity, $c = 342.8$ m/s (as previously calculated from experiments presented in Part 1 of this study), defined the acoustic wavenumber, k_1, hence

$$\Re\{F_n\} = F_0 \cos(k_1 x_{1_n}) \tag{32}$$

and

$$\Im\{F_n\} = F_0 \sin(k_1 x_{1_n}), \tag{33}$$

where $F_0 = 1$ N, and $k_1 = 2\pi f_n/c$. In this way, a travelling wave was simulated, as illustrated in Fig. 8. As can be seen, as one progresses along the panel (in the x direction) each line of nodal harmonic forces has a phase which will lag behind the previous line of nodal forces according to the distance from the edge of the panel, i.e., at $x_1 = 0$. Therefore, for each harmonic solution

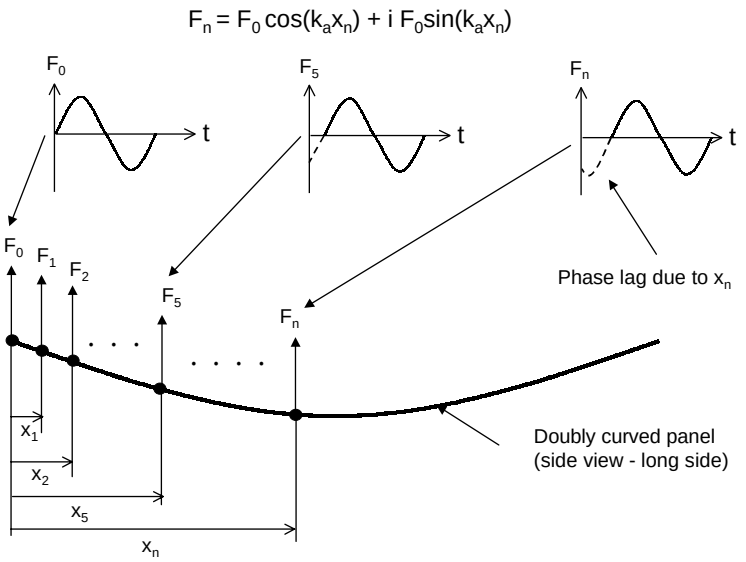

Fig. 8. Illustration of the simulated travelling wave loading applied to the FE model. The phase of the individual line of nodal loads was calculated according to the nodal line location and acoustic wavenumber (defined by the centre frequency in the solution loop).

where the frequency is kept constant, a travelling wave is simulated by virtue of this phase difference between adjacent lines of nodal force. The concept is further illustrated in Fig. 9, where the FE model of panel 1 is shown with the real part of the nodal forces shown for the frequency band centred on, $f_c = 240$ Hz. The real part of the nodal forces is shown (a) in-phase, (b) with a 20° phase lag, (c) with a 40° phase lag, and finally (c) with a 80° phase lag with respect to the initial phase angle. The solution process employed in ANSYS is illustrated in the flowchart in Fig. 10. As can be seen, a harmonic solution with five sub-steps is carried out in each frequency band during which the acoustic wavenumber was kept constant. Following this, the acoustic wavenumber is re-calculated according to the next centre frequency, and the load is re-applied and the harmonic solution obtained. The results are output in terms of the strain transfer function (in $\mu\varepsilon/N$) versus the sub-step frequency values for each strain gauge location.

The strain PSD was obtained by first calculating the strain transfer function in terms of pressure, taking the absolute value and squaring, before finally multiplying by the measured pressure spectrum, $S_{pp}(f)$ obtained from the experiments (see Fig. 2)

$$S_\varepsilon = \left| \frac{\mathbf{H}_\varepsilon(f)}{(F_0 N/A)} \right|^2 . S_{pp}(f), \tag{34}$$

where $\mathbf{H}_\varepsilon(f)$ is the strain transfer function obtained from the FE model (in terms of force), N is the total number of nodes on which the unit force, F_0, was applied, and A is the panel surface area.

The results of the finite element analysis for gauge gi4 on panel 2 are shown in Fig. 11. Here, a comparison has been made between the predicted (FE) and measured strain power spectral density at the five overall sound pressure levels. The predicted response is almost entirely in the first bending mode, with very little contribution evident from other modes, which was also found

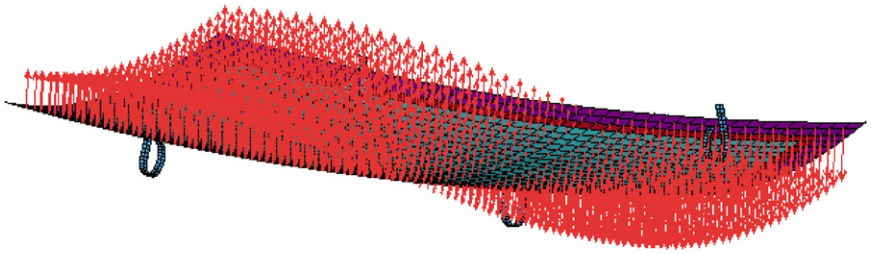

(a) Panel 1, $f = 240$ Hz

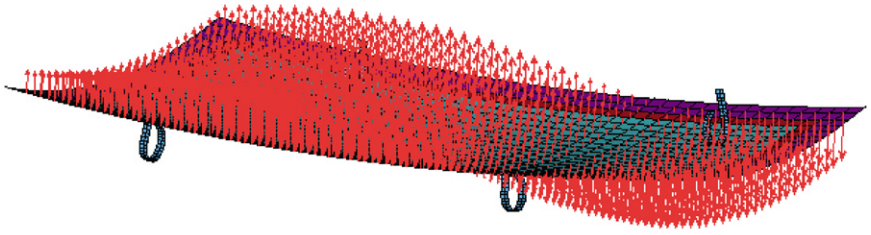

(b) Panel 2, $f = 340$ Hz

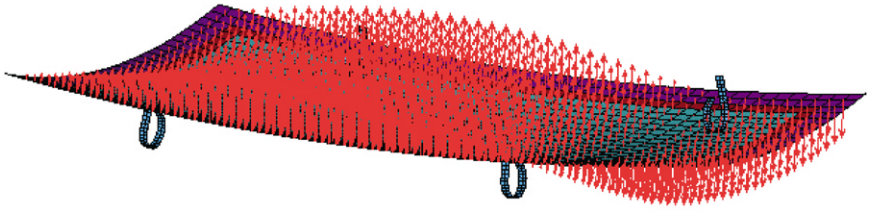

(c) Panel 3, $f = 440$ Hz

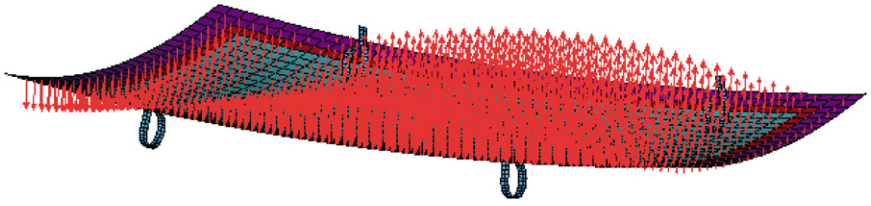

(d) Panel 4, $f = 540$ Hz

Fig. 9. Finite element model of the four doubly curved panels with the travelling wave applied (four different wave frequencies shown): (a) panel 1, $f = 240$ Hz; (b) panel 2, $f = 340$ Hz; (c) panel 3, $f = 440$ Hz; and (d) panel 4, $f = 540$ Hz.

to be the case for panels 1, 3, and 4. The measured response shows a contribution from the second, and in some cases, the third mode. The FE predicted response compares very well with the measured response, and it appears that the FE method under-predicts in the majority of cases when one compares the maximum resonant responses. The r.m.s. strain levels were calculated and compared with the measured r.m.s. responses over the same frequency bandwidth (47–550 Hz). The results for each of the four panels are shown in Figs. 12 and 13. As can be seen, the FE

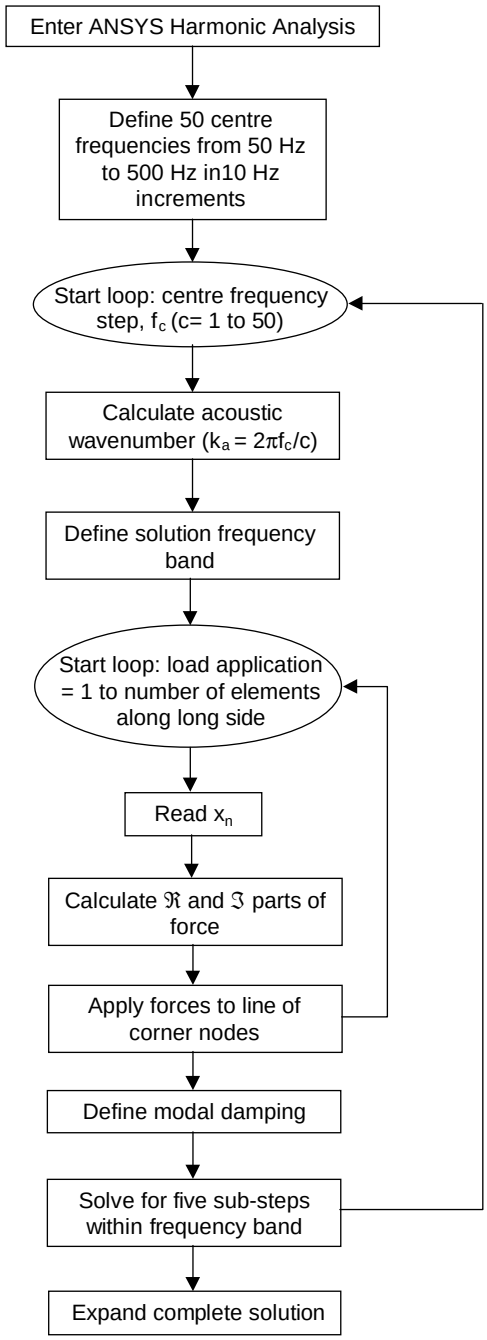

Fig. 10. Flowchart illustrating the harmonic analysis solution process used in ANSYS to simulate travelling acoustic waves at frequencies from 47 to 550 Hz).

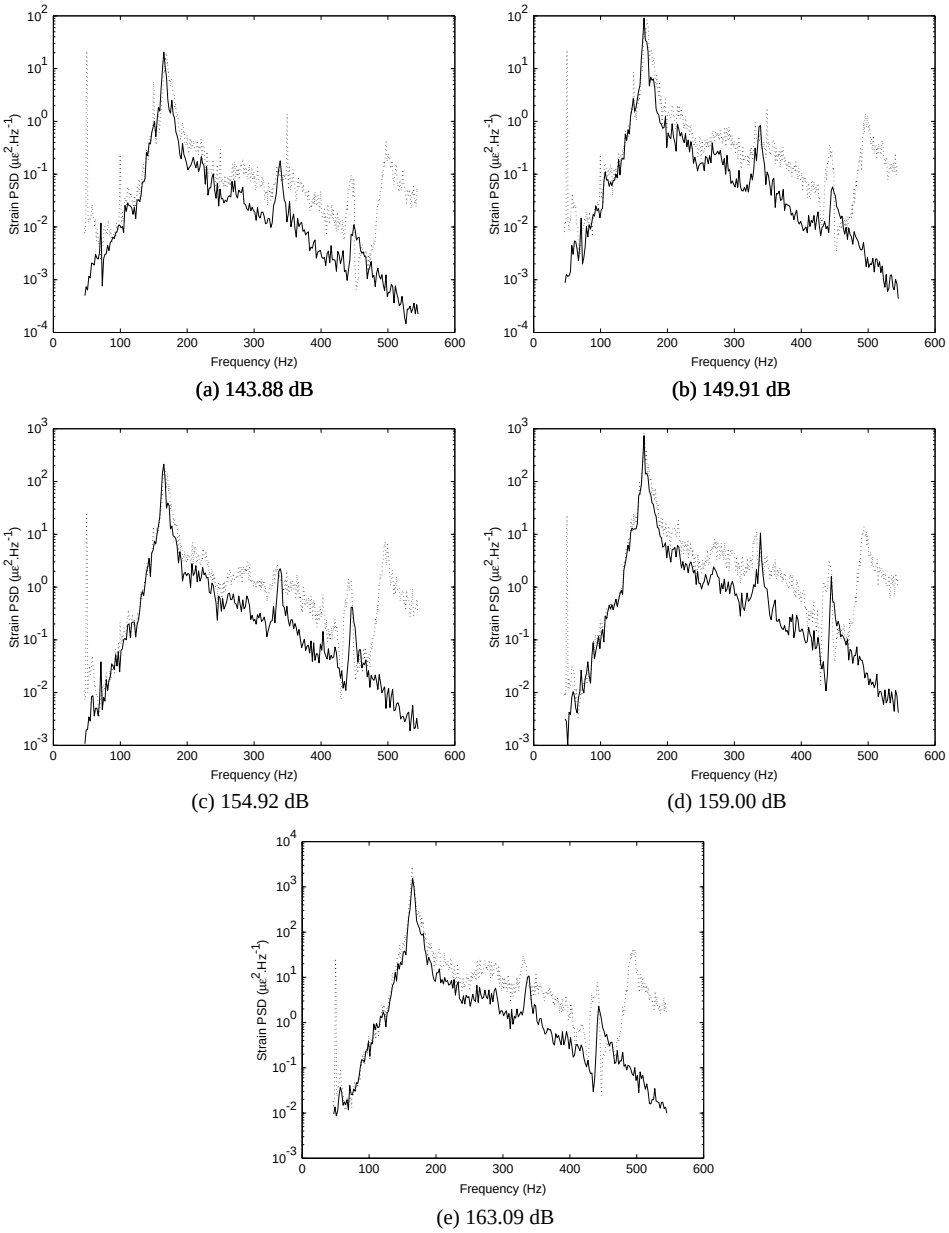

Fig. 11. Comparison of predicted FE (–) and measured (- -) strain PSD for inner centre gauge gi4 (x-wise), panel 2: (a) 143.88 dB; (b) 149.91 dB; (c) 154.92 dB; (d) 159.00 dB; and (e) 163.09 dB.

method resulted in a consistent under-predicted r.m.s. strain response with the majority of the results falling within a 30% confidence limit. The best results were obtained for panels 1 and 2, which was also found to be the case for the s.d.o.f. analysis. For panel 4, the prediction for the outer centre gauges, go4 and go5, gave the worst results. From the plot of the strain PSD, it is

clear that for gauge go4 this can be attributed to a higher mode predominating the response and therefore resulting in a higher r.m.s. value compared to the FE prediction, where there was found to be little response from higher modes. In the FE analysis, the first four non-rigid-body modes were included in the harmonic response, and damping values for each of these modes were included. It is therefore unclear why higher modes are not as apparent in the FE results compared with the measured response. However, the agreement between the experimental results and predicted response was very good for the fundamental mode in all cases, and in some cases such as for gauge gi4 on panel 2 (Fig. 13), the agreement for the higher modes was reasonable. One possible explanation for the higher mode disagreement could be that in the PWT there was some asymmetric excitation across the width of the panel (i.e., from the top to the bottom of the aperture), which could have been enough to excite the higher modes which have nodal lines running along the length of the panel. Since the excitation in the travelling wave method adopted in the FE calculations was constant in phase across the width of the panel (y direction), any modes with nodal lines along the length of the panel would not have been excited. In any case, it is clear from the FE results that the travelling wave method works well for analysing the response of structures to random acoustic excitation.

There is certainly potential for using the travelling wave method in the FE analysis to study the response to various loading spectra, including spectra with discrete tones such as would be found in the duct of an engine intake. Once the harmonic analysis has been carried out and the transfer function obtained, it is a simple matter to find the response to different loading spectra. In addition, it would also be worthwhile investigating the effects of changing various panel design parameters and boundary conditions on the response to random acoustic excitation.

5. Summary

In this paper, three methods used to predict the dynamic response of the doubly curved sandwich panels to random acoustic excitation have been presented. The first method, which combines the classical s.d.o.f. approach with the finite element method, was fully investigated. Three estimates of the spatial characteristics of the pressure loading were used and the results indicated that the Miles [11] approach of a uniform pressure loading resulted in a gross underestimation, while the unit joint acceptance approach (i.e., where the spatial characteristics of the pressure loading exactly match the structural mode shape) resulted in an overestimation. A more accurate estimate of the joint acceptance was formulated by using the results from the FEA modal analysis to calculate the integral of the resonant response mode shape, and by considering the spatial characteristics of the pressure loading to be a series of travelling waves. The resulting estimates compared very well with the measured r.m.s. strain when the latter had been scaled according to the percentage contribution of the fundamental mode to the overall response.

Blevins' normal mode method was also used to predict the response [6]. This method is an extension of the Miles approach which can be used for higher modes and complex shapes. In this study, the mass-weighted mode shape approximation proposed by Blevins [6] was used, which is very similar to the unit joint acceptance approximation described above. The results were very similar to those found using the s.d.o.f. method with unit joint acceptance (Case 2), i.e. an over-estimation. Comparisons have also been made between the calculated joint acceptance using the

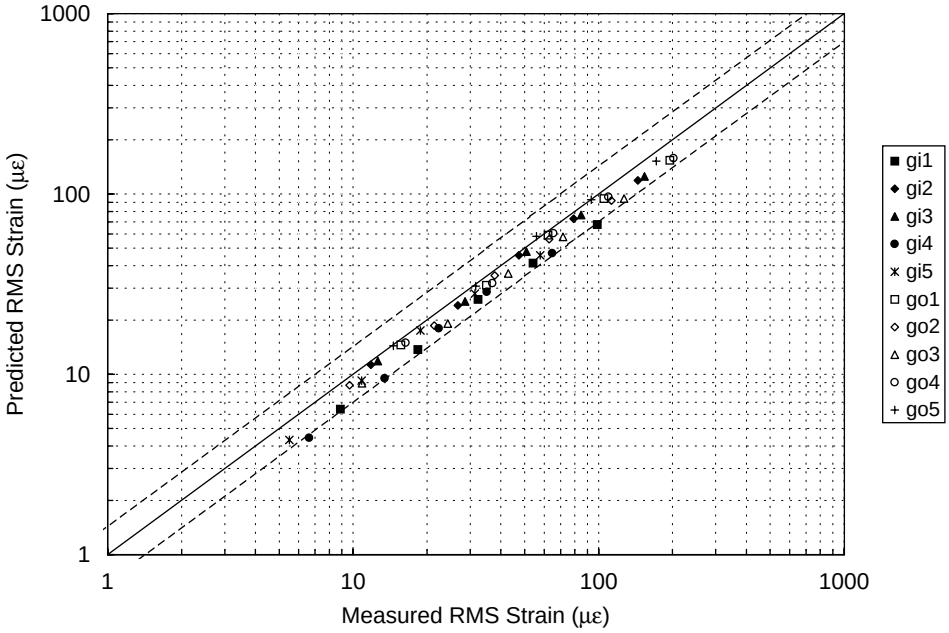

(a) Panel 1

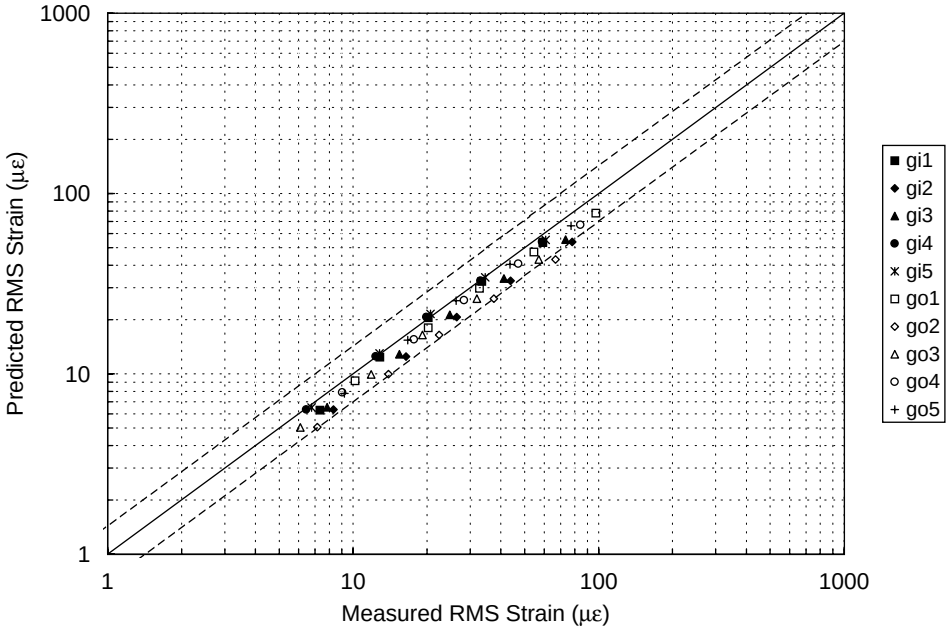

(b) Panel 2

Fig. 12. Comparison of measured and predicted r.m.s. strain for panels 1 and 2 using the finite element method. Overall r.m.s. value calculated between 47 and 550 Hz: (a) panel 1 and (b) panel 2.

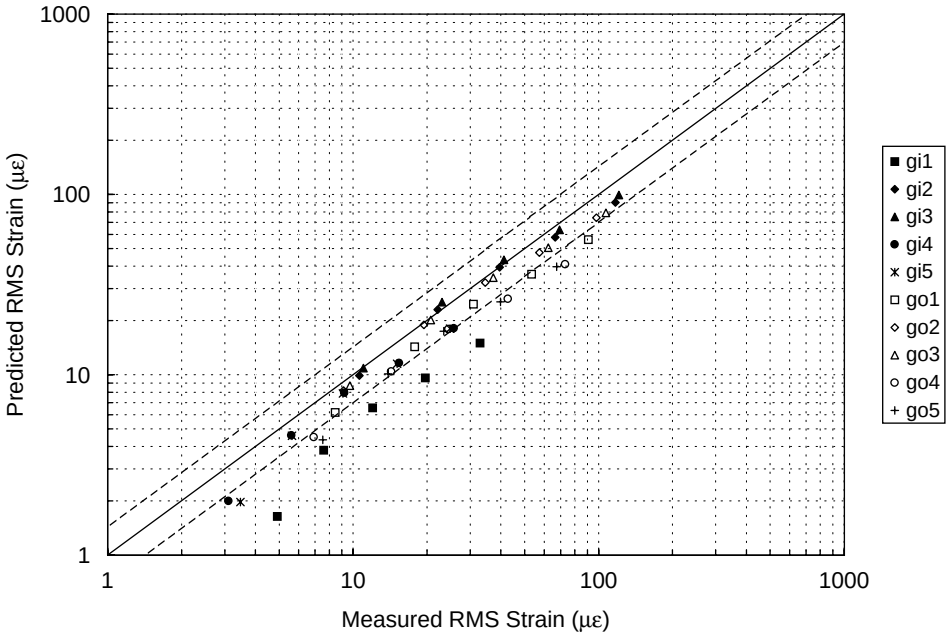

(a) Panel 3

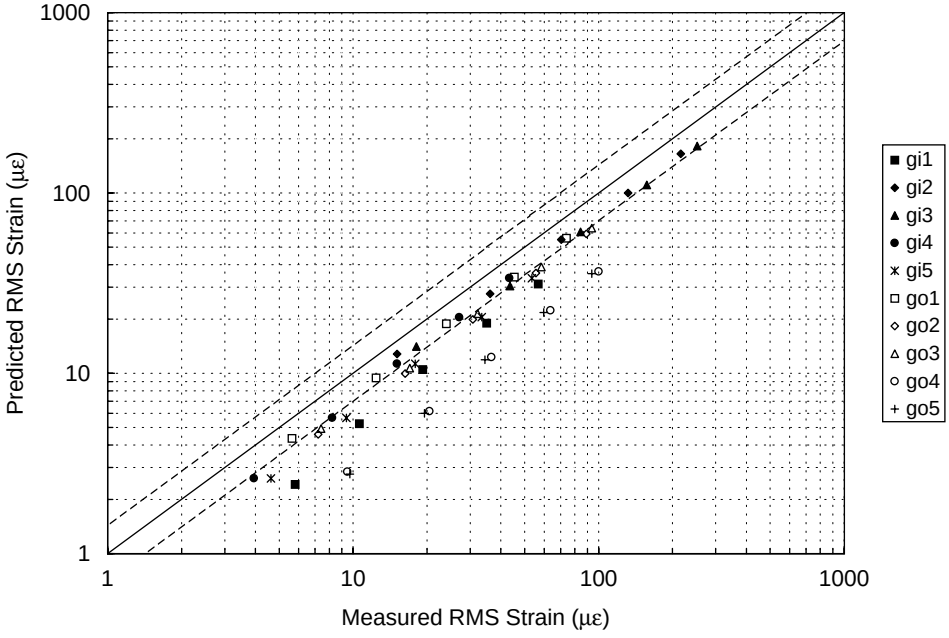

(b) Panel 4

Fig. 13. Comparison of measured and predicted r.m.s. strain for panels 3 and 4 using the finite element method. Overall r.m.s. value calculated between 47 and 550 Hz: (a) panel 3 and (b) panel 4.

method of the present study (Eq. (26)), and the one-dimensional joint acceptance proposed by Blevins [6]. Although the one-dimensional joint acceptance proposed by Blevins would lead to improved estimates of the response of the doubly curved sandwich panels used in the present study, it could not be used in practice because it relies on the sinusoids to model the structural response. This was not feasible due to the non-conventional boundary conditions used to secure the panels in the PWT, which lead to a more complicated mode shape.

For the finite element analysis, the chamfered edge finite element models were used [8], and the spring supports used in the PWT were modelled. In order to model the response to random acoustic excitation, the approach of finding the unit transfer function and multiplying by the pressure PSD was adopted. The unit transfer function was found by conducting a series of harmonic analyses with a simulated travelling wave load on the nodes of the panel. Solutions were found at each frequency where the spatial characteristics of the travelling wave were calculated and the unit force loads applied before each solution step. The results compared very well with the measured response in terms of both the PSD and r.m.s. strain response, although for the former, the higher modes found during measurement were not as apparent from the FE calculations.

In conclusion, the present work has demonstrated that the current approach adopted in the design guides [1], i.e., the Miles equation, yields a very low theoretical prediction when the modes of vibration of the panel include an out-of-plane rigid-body translation. In this instance, the s.d.o.f. method described in this paper can provide very good theoretical predictions when the applied loading distribution can be approximated with simple analytical expressions, and the mode shape can be described using results from a finite element modal analysis. On average, the predicted r.m.s. strains appear to be greater than the measured r.m.s. strains by a factor of about 1.5, although in some cases the method is only in error by about 10%, and in other cases the method under-predicts the r.m.s. strain. However, it must be noted that these comparisons do not take into account experimental uncertainties in the measured strains, damping values, or pressure spectrum. In addition, it has been shown that the finite element method can be used successfully to predict the response when the applied loading distribution is modelled as a series of travelling waves. It is clear from the present work that the estimation of the spatial distribution of the pressure loading is a key input to the methods presented here, and future research into the development of an improved estimation of this distribution, possibly using computational aero-acoustics methods, is essential if predictions are to be further improved.

Acknowledgements

This work was supported by the Engineering and Physical Sciences Research Council (EPSRC).

References

[1] Engineering Sciences Data Unit, Vibration and acoustic fatigue, ESDU Design Guide Series, Vols. 1–6, ESDU International, London.

[2] B.L. Clarkson, Stresses in skin panels subjected to random acoustic loading, The Aeronautical Journal of the Royal Aeronautical Society 72 (1968) 1000–1010.

[3] J.E. Sweers, Prediction of response and fatigue life of honeycomb sandwich panels subjected to acoustic excitation, in: W.J. Trapp, D.M. Forney (Eds), Acoustical Fatigue in Aerospace Structures, Syracuse University Press, Syracuse, NY, 1964, pp. 389–402.
[4] J. Soovere, Random vibration analysis of stiffened honeycomb panels with beveled edges, American Institute of Aeronautics and Astronautics Journal of Aircraft 23 (6) (1986) 537–544.
[5] B.L. Clarkson, Review of sonic fatigue technology, NASA Technical Report CP-4587, 1994.
[6] R.D. Blevins, An approximate method for sonic fatigue analysis of plates and shells, Journal of Sound and Vibration 129 (1989) 51–71.
[7] P.R. Cunningham, R.G. White, Dynamic response of doubly curved honeycomb sandwich panels to random acoustic excitation. Part 1: Experimental study, Journal of Sound and Vibration 264 (3) (2003) 579–603, this issue.
[8] P.R. Cunningham, R.G. White, G.S. Aglietti, The effects of various design parameters on the free vibration of doubly curved composite sandwich panels, Journal of Sound and Vibration 230 (3) (2000) 617–648.
[9] L. Meirovitch, Elements of Vibration Analysis, McGraw-Hill, New York, 1986.
[10] D.E. Newland, An Introduction to Random Vibrations, Spectral and Wavelet Analysis, Longman Scientific & Technical, London, 1993.
[11] J.W. Miles, On structural fatigue under random loading, Journal of the Aeronautical Sciences 21 (1954) 753–762.
[12] P.R. Cunningham, Response Prediction of Acoustically-Excited Composite Honeycomb Sandwich Structures with Double Curvature, Ph.D. Thesis, University of Southampton, 2001.
[13] J.N. Little, L. Shure, For Use with MATLAB, Signal Processing Toolbox, Vol. 95, The Math Works Inc., Natick, MA, Chapter 2.